5-4-2015

Polymer Based Micro Scale Force Sensing Cantilevers for Biosample Manipulation and Measurements

Hasan S. Fiaz
University of Connecticut - Storrs, hasan.fiaz@uconn.edu

Polymer Based Micro Scale Force Sensing Cantilevers for Biosample Manipulation and Measurements

Hasan Syed Fiaz

B.S., University of Engineering and Technology, 2012

A Thesis

Submitted in Partial Fulfillment of the

Requirements for the Degree of

Master of Science

At the

University of Connecticut

2015

APPROVAL PAGE

Master of Science Thesis

Polymer Based Micro Scale Force Sensing Cantilevers for Biosample Manipulation and Measurements

Presented by

Hasan Syed Fiaz, B.S.

Major Advisor_____
Kazunori Hoshino

Associate Advisor_____
Quing Zhu

Associate Advisor_____
Guoan Zheng

University of Connecticut

2015

Acknowledgements

All the praises and thanks belong to God Almighty for bestowing His gracious blessings. First and foremost, I would like to express my deepest gratitude to my major advisor, Dr. Kazunori Hoshino. Throughout my time at the Nano and Micro-Scale Optical Imaging and Mechanical Sensing for Biomedical Analysis Laboratory, he has provided strong support in every aspect. He has offered me guidance, encouragement, professional advice and constructive criticism for which I will be extremely grateful. I would like to thank my other committee members, Dr. Quing Zhu and Dr. Guoan Zheng, for their guidance and support.

I also extend an expression of special thanks to my colleagues, Devina Jaiswal, Radhika Shiradkar and Soliman Alhudaithy, for supporting and encouraging me throughout my Master's studies. Words are inadequate to express my gratitude for my family and friends. I like to thank some wonderful people here in University of Connecticut, Meenakshi Sharma, Gagan Sharma, Gil Banton, Leah Ward, Siyuan Dong, Kaikai Guo and Bian Zichao.

More specifically, I would like to dedicate this thesis to my mother, Mrs. Shamim Fiaz, my father, Dr. Fiaz Hussain Shah, and my fiancé, Sana Batool. This work was possible due to their valuable guidance, sacrifices, endless support, understanding and love.

Table of Contents

List of Figures

List of Tables

Abstract

Cancer has long been one of the major causes of death worldwide. It has been studied and known that cancer can distort the mechanical properties of cells. Recent advancement in biomechanics refers to a significant relationship between cell stiffness and cell condition. Mechanical stiffness can be used to identify abnormal cell populations as in tumors in detecting cancer and can be employed as a diagnostic parameter for various diseases. In this study, we introduced micro fabrication technology to develop polymer based cantilevers integrated with thin chromium film resistor as a transduction scheme. Cantilevers are beam like micro structures anchored only at one end with the other end freely suspended. When a force or load is applied along the length of the cantilever or at the free end, the cantilever bends and stresses are induced on the cantilever surface which changes the resistance of thin chromium film resistor. A custom built amplifier allows for a sensitive response to the deflection.

Cantilevers with different dimensions and stiffness were calibrated. The force detection was in the range of 5-500μN. The cantilever based sensor was used to find the stiffness of an elastic Polydimethylsiloxane (PDMS) micro pillar of diameter 200μm and height 100μm. The purpose of this experiment was to realize cantilevers to manipulate an elastic micro structure mimicking cantilever manipulation with cluster of cells or cancer spheroid of comparable size. A PDMS film containing micro pillars was fabricated using UV lithography and soft lithography techniques. When the cantilever was moved against the PDMS micro pillar with the help of mechanical stage displacement, the cantilever deflected and the PDMS micro pillar displaced as well. Using the measurements and calculations from cantilever calibration and cantilever manipulation with elastic PDMS micro pillar, the stiffness of elastic PDMS micro pillar of diameter 200μm and 100μm was measured which was 0.97 Nm^{-1}.

The cantilever based sensor was also used to measure force in cancer cell manipulation. The purpose of this experiment was to show the capability of handling cells. A cell holding device was fabricated using UV lithography and soft lithography techniques. The cell holding device was a PDMS film that consisted of a circular well of depth 100μm and PDMS micro pillars of diameter 300μm and height 100μm. MCF-7 cancer cells were centrifuged and an aggregation of MCF-7 cancer cells was pasted onto the circular well of the PDMS film. Using the measurements and calculations from cantilever calibration and cantilever manipulation with aggregation of cancer cells, the stiffness of the whole system consisting of the PDMS film with PDMS micro pillars and aggregation of MCF-7 cancer cells was measured which was in the range 2.0-2.3 Nm^{-1}. A force range of 5-90μN was detected and applied which resulted in indentation of aggregation of MCF-7 cancer cells seen under the microscope.

These cantilever based sensors are compatible to explore the stiffness of cluster of cancer cells or cancer spheroids. These findings suggest that the polymer based micro scale force sensing cantilevers designed, fabricated and tested in this study can be used for biosample manipulation and measurements.

Chapter 1

Introduction

1.1 Background and motivations

The inception and growth of some human disease states can be greatly correlated with the mechanical properties of cells. The physiological functions of the cells can be disrupted by deviations in the mechanical properties resulting in diseases like malaria (Lim et al., 2006). On the contrary, diseases may cause changes in the morphological and mechanical properties of individual living cells such as cancer (Li et al., 2008). Cell mechanics can play an essential role in the study of human diseases and moreover assist in differentiating diseased cells from healthy cells (Crick et al., 2007).

Cancer has long been one of the major causes of death and is currently held responsible for about 25% of all deaths worldwide (Jemal et al., 2005). It is predicted that by 2020 there will be about 15 million new cases of cancer annually (Lee et al., 2007). Since it has been studied and known that diseases like cancer can distort the mechanical properties of cells, this will likely aid in the early detection of cancer (Lee et al., 2007). Furthermore, examining the mechanical properties of cancer cells may help to better understand the physical mechanisms responsible for cancer metastasis. This can lead to the development of novel strategies for the prevention and diagnosis of cancer (Li et al., 2008).

Recent advancement in biomechanics has lead to the possibility of exploring mechanical influences on cells. Still, there are very few experimental techniques proficient of determining cellular mechanical properties (Guck et al., 2005). Historically, the most common and prevailing

technique has been micropipette aspiration (Hochmuth, 2000). Others have used magnetic bead rheology (Wang et al., 1993), microneedle probes (Zahalak et al., 1990), microplate manipulation (Thoumine and Ott, 1997), acoustic microscopes (Kundu et al., 2000), arranging micro fabricated sieves (Carlson et al., 1997) and manipulation of beads attached with cells by optical tweezers (Sleep et al., 1999). Lincoln et al. were the first to employ an optical stretcher to investigate the deformability of malignant and normal human breast epithelial cells (Lincoln et al., 2004). These techniques mentioned experience considerable difficulties in common applications. The reasons are low cell throughput which leads to poor statistics, mechanical contact of the probe leading to active cellular response and adhesion, and non-physiological handling leading to measurement artifacts (Guck et al., 2005).

In the past two decades, the field of Micro-electromechanical systems (MEMS) and micro fabrication has grown tremendously (Hopcroft et al., 2005). It has led to the emergence of the field of cantilever based sensing. The study of cantilever based sensors followed the development of two autonomous technologies. The first part is the invention of atomic force microscopy (AFM) in 1986. Binning and Quate from Stanford University used a scanning tunneling microscope (STM) to measure the motion of a cantilever beam with an extremely small mass (Binning et al., 1986). They were able to measure the force between the cantilever tip and the sample surface. The force required to deflect the cantilever to a measurable distance can be as small as 10^{-18} N. Binning moreover discussed that micro fabrication would be needed in order to make the cantilevers with a mass less than 10^{-10} kg and a resonant frequency greater than 2 kHz (Binning et al., 1986).

The other fundamental technology is micro fabrication. In 1990 at Stanford University, Albrecht et al. realized micro fabricated cantilevers with integrated tips for measurements in

AFM (Albrecht et al., 1990). Several methods to fabricate SiO_2 and Si_3N_4 based micro cantilevers were investigated. In 1991, Wolter et al from IBM developed a batch process for the micro fabrication of single crystal silicon force sensors (Wolter et al., 1991). In the mid 1990s based on the technologies developed for AFM, studies on micro scale cantilevers for sensing were introduced initiating the field of cantilever based sensing. Since then the research area has grown rapidly. Cantilevers with integrated read-out started to appear in late 1990s. The integrated read-out aids in the development of compact devices that can even operate in non-transparent environments (Boisen et al., 2011). For example, in 2000, piezoresistive cantilevers for surface stress sensing were reported demonstrating the realization of dense array of sensors with a compact read-out technique (Boisen et al., 2000).

Micrometer-sized cantilevers are sensitive, label-free, inexpensive, portable, highly parallel and fast sensors drawing attention from applications such as point of care (POC) diagnostics, homeland security and environmental monitoring (Boisen et al., 2011). Cantilevers are very interesting significant research tools which offer the possibility to measure quantities and phenomena that are very difficult to achieve using other methods. The sensors are versatile, measuring phenomena like changes in surface stress, temperature and mass (Boisen et al., 2011).

AFM has also been used to determine the elastic properties of cells (Mahaffy et al., 2000; Rotsch et al., 1999). Further, AFM has been implemented to examine the mechanical properties of *ex vivo* cancer cells acquired from patients (Cross et al., 2007). Lekka et al. investigated the elastic properties of normal human bladder epithelial cells and cancerous ones by executing AFM indentation on these cells (Lekka et al., 1999).

All the techniques mentioned here hint and refer to a significant relationship between cell stiffness and cell condition. Executing AFM indentation, Lekka et al founded that normal cells were stiffer than cancer cells by an order of magnitude (Lekka et al., 1999). Adopting the technique of micropipette aspiration, researchers detected a 50% reduction in elasticity of malignantly transformed fibroblasts as compared to their normal counterparts (Ward et al., 1991). Employing an optical stretcher to investigate the deformability of malignant and normal human breast epithelial cells, Lincoln et al found that the malignant cell could stretch five times more than the normal cell (Guck et al., 2005; Lincoln et al., 2004). *In vitro* investigations carried out by various techniques have shown that some cancer cells were softer and less stiff than normal counter cells (Lekka et al., 1999; Guck et al., 2005; Lincoln et al., 2004; Thoumine et al., 1997; Suresh et al., 2007). Depending on different techniques used to investigate mechanical properties of cells, mainly cancerous cells are less stiff and less resistant to flow, in response to respective techniques.

However, tumors differ in mechanical stiffness than individual cancer cells and normal tissue. Krouskop et al. used elastography (ultrasound medical imaging modality that maps the elastic properties of soft tissue) to find the stiffness of normal prostate tissue and cancerous prostate tissue. They founded that normal prostate tissue had a modulus lower than prostate cancerous tissue (Krouskop et al., 1998). Using the same technology, Hoyt et al. revealed that the viscosity parameter for cancerous prostate tissue was greater than that derived from normal tissue by a factor of approximately 2.4. It was also determined that a difference existed between normal and cancerous prostate tissue stiffness producing an average elastic contrast that increased from 2.1 at 0.1 Hz to 2.5 at 150 Hz (Hoyt et al., 2008).

In summary, mechanical stiffness can be used to identify abnormal cell populations as in tumors in detecting cancer and can be employed as a diagnostic parameter for various diseases (Li et al., 2008). The mechanical stiffness and force detection range of individual cancer cells and tumors vary so it is important to develop cantilevers which can sense a wide force range in micro scale.

1.2 Aims of thesis

The aim of this thesis is the development of micrometer-sized cantilevers that can sense force in micro scale. The design and fabrication of these cantilevers is carried out using the technology of micro fabrication. Micro fabrication allows the fabrication of versatile cantilevers and addition of integrated functionality. Employing these micro scale force sensing cantilevers, the stiffness of elastic micro structures can be explored by cantilever manipulation.

The main goal of this thesis is to explore the stiffness of cluster of cancer cells. This can help in identifying abnormal cell populations as in tumor in detecting cancer. Figure 1.1 below shows the schematic view of cluster of cancer cells and cantilever. Cantilevers are beam like micro structures anchored only at one end with the other end freely suspended. When a force or load is applied along the length of the cantilever or at the free end by moving the cantilever against a cluster of cancer cells, the cantilever deflects and stresses are induced on the cantilever surface which can be detected. The detection is done by a particular transduction arrangement allowing for a sensitive response to deflection. The deflection of the cantilever can be measured under an optical microscope. The spring constant beam or stiffness of the cantilever (S) is characterized by the physical dimensions of the cantilever and mechanical specification of the cantilever material. This is discussed in chapter 2. The force (F) can be calculated by the relation

of deflection and spring constant beam. The manipulation of the cantilever with the cluster of cancer cells also causes indentation of cells. This indentation is investigated using an optical microscope or using measurements of cantilever manipulation. The stiffness of elastic micro structures especially of cluster of cancer cells can be explored.

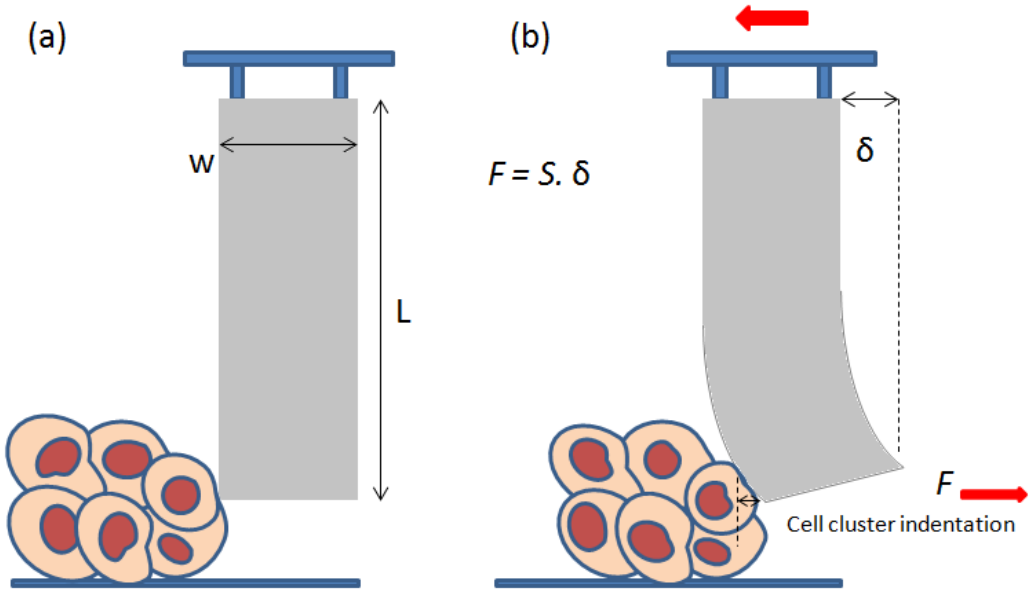

Figure 1.1 Schematic of cantilever and cluster of cancer cells

1.3 Thesis outline

A brief outline of the thesis is as follows. Chapter 1 provides an overview of the background relevant to this research. It explains about the distortion of mechanical properties of cells caused by cancer and presents the methods that have been used to investigate cellular mechanics. It also describes the emergence of cantilever based sensing and why it is important to develop micro scale force sensing cantilevers as they are potential sensors for measuring mechanical stiffness. Chapter 2 presents the theoretical background of cantilevers and explains the mechanics of cantilevers. The proposed design, transduction scheme and material for the

fabrication of cantilever based sensors are also mentioned. Chapter 3 provides a detailed account of the fabrication process of polymer based micro scale force sensing cantilevers and the materials and methods involved. Chapter 4 describes the experimental setup used to conduct experiments, results of experiments and related discussion. Chapter 5 provides the conclusion drawn from this research and future directions.

Chapter 2

Polymer based cantilevers

2.1 Mechanics of cantilever (Adapted from Zhang and Hoshino, 2014)

Structural analysis of a cantilever is the basic subject to investigate the mechanical characteristics such as force, stress, strain, moment and radius of curvature. The sensitivity of a cantilever is dependent on the physical dimensions and alters with mechanical specifications including Young's modulus and Poisson's ratio. Some basic mechanical characteristics are as follows:

$$\text{Stress } (\sigma): \quad \sigma = F/A \tag{1}$$

$$\text{Strain } (\varepsilon): \quad \varepsilon = \Delta L/L \tag{2}$$

$$\text{Young's modulus } (E): \quad E = \sigma/\varepsilon \tag{3}$$

Young's modulus is a measure of the material stiffness and is defined as the ratio of the stress to the strain. It is a material characteristic defined independent of the dimensions of the structure.

2.1.1 Stress distribution

Figure 2.1 below shows a simple model of a mechanical cantilever. Dimensions are width 'w', thickness 't' and length 'L'. Let us consider a concentrated transverse force '*F*' is applied at the free end of the cantilever. In MEMS, this situation is encountered frequently. This transverse force introduces longitudinal strains. The distribution of longitudinal stress is first described qualitatively (Figure 2.2). The torque distribution through the length of the beam is non-uniform

under a transverse force loading; it is zero at the free end and reaches a maximum at the fixed end. At any cross section, the signs of the longitudinal stresses change across the neutral axis. The magnitude of the stresses at any point on the cross section is linearly proportional with respect to the distance to the neutral axis. The magnitude of the maximum stresses associated with individual cross sections change linearly with respect to the distance to the free end, reaching a section wide maximum at the top and bottom surfaces. Because of these reasons, piezoresistors are commonly found near the fixed end and on the surface of the cantilever.

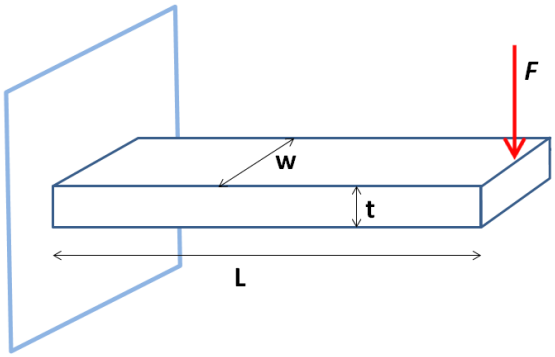

Figure 2.1 Model of cantilever (Redrawn from Zhang and Hoshino, 2014)

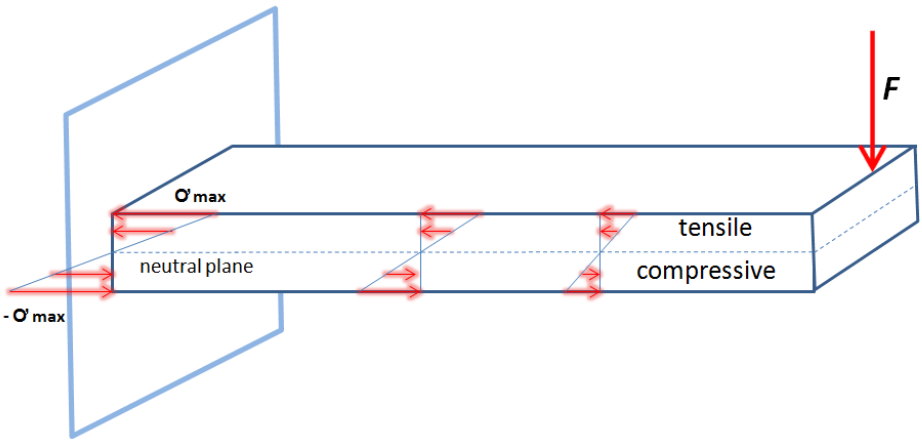

Figure 2.2 Stress distribution in an uniform and symmetric cantilever beam

For quantitative analysis, let us consider a part *l* of the cantilever separated at imaginary cross section *A* at *x* shown below in Figure 2.3.

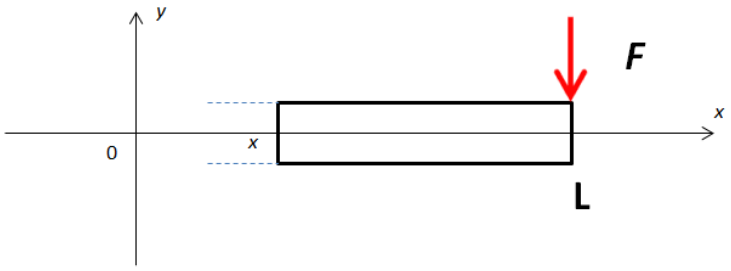

Figure 2.3 Part of cantilever separated at imaginary cross section (Redrawn from Zhang and Hoshino, 2014)

Now all the forces to support the part come from the cross section. Since part *l* is in mechanical equilibrium, the external forces and the moments of the external forces must satisfy equilibrium equations.

(i) The sum of all the external forces is zero. The force to counter force *F* is a shear force *–F* at the cross section and its intensity is independent of the length of *l* (Figure 2.4).

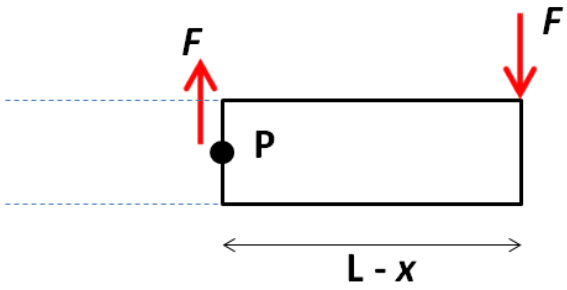

Figure 2.4 Force equilibrium (Redrawn from Zhang and Hoshino, 2014)

(ii) The sum of moments of the external force is zero. The external force F produces moment M_F about axis a in Figure 2.4.

$$M_F = F.(L - x) \quad (4)$$

The moment to counter M_F is created by a distribution of normal stresses $\sigma(y)$ at A as shown in Figure 2.5. Moment M produced by $\sigma(y)$ about axis p must cancel the moment M_F induced by external force.

$$M_F + M = 0 \quad (5)$$

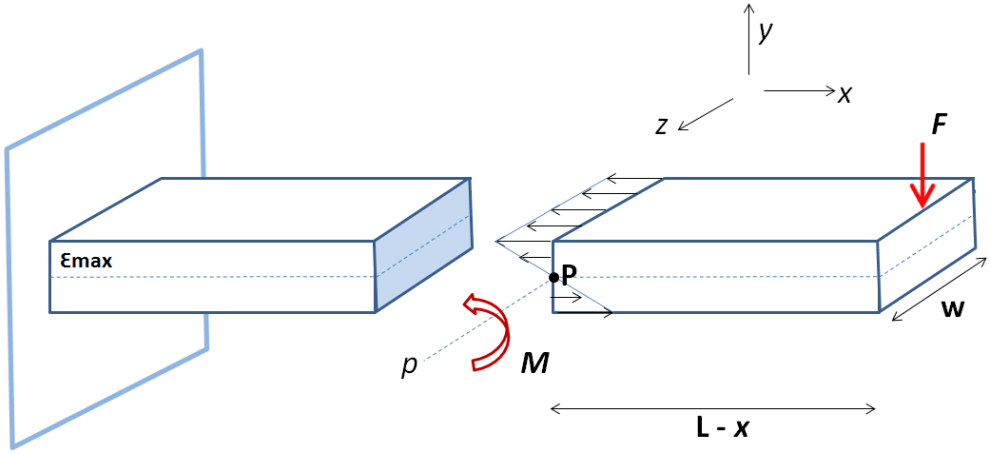

Figure 2.5 Moment equilibrium: moment induced by stress distribution

Since the net force in x direction is zero, the integration of $\sigma(y)$ along the surface should also be zero. When we assume $\sigma(y)$ is linearly distributed along y, $\sigma(y)$ is expressed as:

$$\sigma(y) = k \, . \, y \quad (6)$$

M is the moment produced by $\sigma(y)$ about p:

$$M = \int_{-t/2}^{t/2} y \, . \, w. \, \sigma(y) \, .dy = k \int_{-t/2}^{t/2} w y^2 \, . \, dy \quad (7)$$

In order to simplify the following discussion, we define term I as (Figure 2.6):

$$I = \int_{-t/2}^{t/2} wy^2 \, . \, dy = (wt^3) / 12 \qquad (8)$$

The term I is called the second momentum of area.

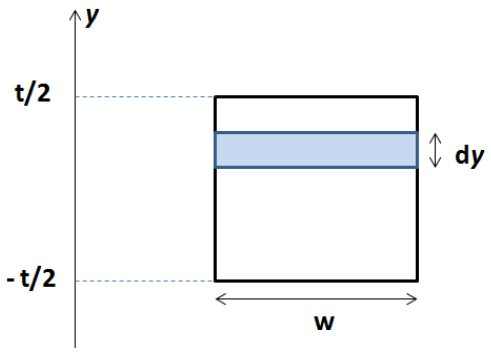

Figure 2.6 Integration to show the second momentum of area (Redrawn from Zhang and Hoshino, 2014)

Using I, the moment M is simply expressed as:

$$M = k \, . \, I \qquad (9)$$

Using (6), the stress distribution becomes:

$$\sigma(y) = (M / I) \, y \qquad (10)$$

Comparing equations (6) and (10) and using (5), we find,

$$k = (M / I) = - (M_F / I) \qquad (11)$$

Putting Eq(4) into Eq(11), we get,

$$\sigma(y) = [F \,.\, (L - x) / I\,]\, y \qquad (12)$$

As we see in (12), the stress becomes larger as the cross section gets closer to the fixed end, meaning x which is the distance from fixed end becomes smaller or ($L - x$) becomes larger.

2.1.2 Cantilever bending

The relationship between a normal stress and a strain is given in Equation (3). The stress distribution in a beam can be correlated to the distribution of strain which leads to cantilever deflection or bending.

Using Eq(3) and Eq(10),

$$\varepsilon(y) = \sigma(y) / E$$

$$\varepsilon(y) = (M / E\, I)\, y \qquad (13)$$

Let us consider a small slice of the beam with the length dx at $y = 0$ shown in Figure 2.7.

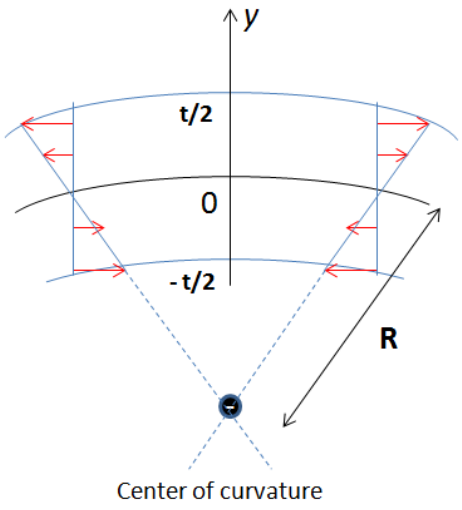

Figure 2.7 Radius of curvature (Redrawn from Zhang and Hoshino, 2014)

As shown above in Figure 2.7, the slice is deformed following the linear strain distribution. The length at y which is longest at t/2 and shortest at –t/2 is given as:

$$dl(y) = (1 + \varepsilon(y)) \, . \, dx = (1 + (M / EI) \, y) \, . \, dx \qquad (14)$$

The center of curvature of the beam can be found as the position where $dl(y) = 0$. The center of curvature R becomes:

$$R = - (E \, I) / M \qquad (15)$$

The radius of curvature of a curve $y = y(x)$ is given as:

$$R = (1 + y'^2)^{3/2} / y'' \qquad (16)$$

y' is negligibly smaller than 1 in our model thus,

$$R = 1 / y'' \qquad (17)$$

This is a significant relationship to correlate curvature and bending of the beam. From Eq(15) and Eq(17) we find,

$$y'' = - M / E \, I \qquad (18)$$

Substituting M by using Eqs (4) and (5), the external force can be correlated with beam bending,

$$y'' = - [F(L - x)] / E \, I \qquad (19)$$

By integrating Eq (19) twice and putting fixed end boundary conditions of $y(0) = y'(0) = 0$, we find,

$$y = [F \, x^2(3L - x)] / 6EI \qquad (20)$$

The maximum deflection is at x = L,

$$y_{max} = (L^3 / 3EI) . F \quad (21)$$

Or,

$$F = [(3EI) / L^3] . y_{max} \quad (22)$$

The term $3EI / L^3$ defines the linear relationship between the applied force F and deflection. It is considered as the effective spring constant of the beam at x = L in the y direction. It is the stiffness of the cantilever beam with units of (Nm^{-1}). Using Equation (8) and by using I we get,

$$k_{eff} = [(3EI) / L^3] = [(Ewt^3) / 4L^3] \quad (23)$$

Equation (23) shows that if we know the parameters of the cantilever like width, thickness, length and the Young's modulus of the material the cantilever is made up of, we can assume the stiffness of the cantilever as **$[(Ewt^3) / (4L^3)]$.** By measuring the deflection of the cantilever, we can find the assumed force (F) applied at the free end of the cantilever to cause that particular deflection.

$$\boldsymbol{F = [(Ewt^3) / (4L^3)] . y_{max}} \quad (24)$$

2.1.3 Strain produced at the fixed end of cantilever

As described in the previous section, the maximum stress is experienced at the top and bottom surfaces of the cantilever (tensile and compressive respectively depending on the loading direction at the free end) and is experienced at the fixed end of the cantilever. Figure 2.8 below shows a case study of some points of stresses experienced on a cantilever.

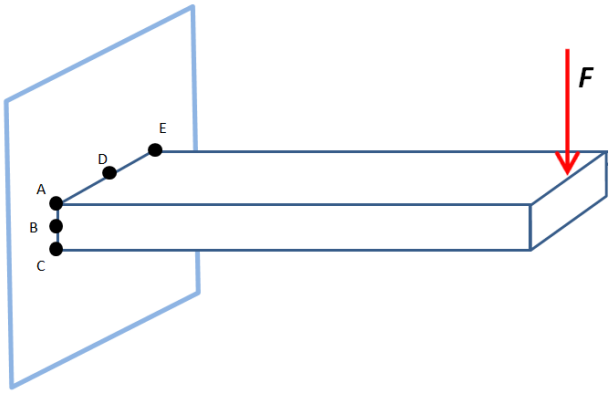

Figure 2.8 Case study of points of stresses on cantilever

Under the case shown in Figure 2.8, a transverse force *F* is applied at the free end of the cantilever. The other end of the cantilever is fixed. The stress at Points A, C, D and E is the greatest and the minimum stress occurs at Point B. Points A, D and E are under tension while Point C is under compression. Point B experiences the minimum or no stress even though it is situated at the fixed end. The reason is it lies directly on the neutral plane and just at the center of the cross section. The maximum stress is experienced at the fixed end when force *F* is applied at the free end on the cantilever. So,

Equation (4) becomes,

$$M = F.\,\mathrm{L} \qquad (25)$$

Equation (10) becomes,

$$\sigma_{max} = [(F.\mathrm{L}) / I\,].y \qquad (26)$$

We will use $y = t/2$ as the stress varies from tension to compression or vice versa with zero stress on the half line of the thickness of the cantilever which is the neutral plane. We will use Equation (8) to use *I*.

Now,

$$\dot{O}_{max} = [(F.L) / (wt^3/12)]. (t/2) \quad (27)$$

By simplifying, we get the magnitude of maximum stress as:

$$\dot{O}_{max} = [(6FL) / (wt^2)] \quad (28)$$

Using Equation (3), we get the magnitude of maximum strain as:

$$\dot{\varepsilon}_{max} = [(6FL) / (Ewt^2)] \quad (29)$$

2.2 Polymer as cantilever material

Researchers are moving aside from conventional silicon-based technologies in the field of MEMS lately and are investigating alternative materials (Hopcroft et al., 2005). In the last two decades, an increasing amount of work has been addressed on the fabrication of polymer based cantilevers. The most valuable advantage of using polymers is that the magnitude of Young's modulus is lower than traditional silicon-based materials by an order of two (Boisen et al., 2011). As mentioned before, the spring constant of a beam (stiffness) is $[Ewt^3/4L^3]$**,** showing that the stiffness is directly proportional to the Young's modulus of the material used to fabricate the cantilever. A lower Young's modulus constitutes to a lower stiffness of the cantilever resulting in increased variation in deflection making the cantilever more sensitive. The stiffness of the cantilever can be further customized by simply changing the composed material. Another significant advantage of using polymers is the comparative inexpensive raw material and fabrication process (Boisen et al., 2011).

2.2.1 SU-8 as a device material

For effective operation, a cantilever requires specific properties. Using conventional silicon-based micro fabrication techniques, it is difficult to make cantilevers with sufficiently low spring constant (stiffness) to accomplish small forces required, as the thinness of the cantilever becomes a limiting factor (Hopcroft et al., 2005). The Young's modulus of silicon is 130-188GPa (Hopcroft et al., 2010). Photo plastic polymers with a low Young's modulus (normally below ~ 5GPa) are an appealing alternative because they can be used to make robust and thick cantilevers with required properties (Genolet et al., 1999). One of these polymers is SU-8.

SU-8 is a negative epoxy-based photoresist which allows the fabrication of chemically and thermally stable, highly cross-linked microstructures with high aspect ratios. The Young's modulus of SU-8 is 2.2 ± 0.1GPa (Gao et al., 2010). It has excellent imaging characteristics and a very high optical transmission above 360nm. It can be spin-coated to thicknesses ranging from below 1µm up to 1mm and the final structures can be defined by standard lithography tools e.g. UV lithography or e-beam lithography. Its low Young's modulus, high mechanical strength, advantageous chemical properties, simpler and inexpensive fabrication process and compatibility with standard lithography makes SU-8 a promising candidate and highly suitable material for the fabrication of cantilever based sensors. Furthermore, micromachining enables a versatile cantilever fabrication process which makes the integration of additional functionality easier and allows a variety of cantilever shapes to be designed. Recently, SU-8 has been used for the fabrication of cantilevers in commercial AFM and with integrated piezoresistive sensors (Hopcroft et al., 2005; Nordstrom et al., 2008; MicroChem SU-8 processing guidelines).

2.3 Sensor read-out principles

The precision of sensing read out schemes (transduction) presents another limiting factor to the overall sensitivity of a cantilever based sensor system. At micro and nano scale, specialized instruments are used to accurately measure the changes in deflection (Zhang and Hoshino, 2014).

Various sensitive displacement sensors have been explored in order to detect minimal cantilever deflection. Some schemes are firm and robust but rather bulky while some are immature but have advantages of being miniature. Optical read-out, capacitive read-out, piezoresistive read-out and interferometry are general transduction methods used for sensing (Boisen et al., 2011).

One interesting transduction arrangement is the use of thin metal film resistors. Thin metal film resistors are deposited near the fixed end and on the surface of cantilevers as maximum stress is induced on those positions. These thin metal film resistors are deposited using variety of vacuum deposition methods referred as physical vapor deposition (PVD). Thin films are deposited by condensation of the vaporized form of the desired film material onto the substrate surfaces. Figure 2.9 below shows the concept of using deposited thin metal film resistors.

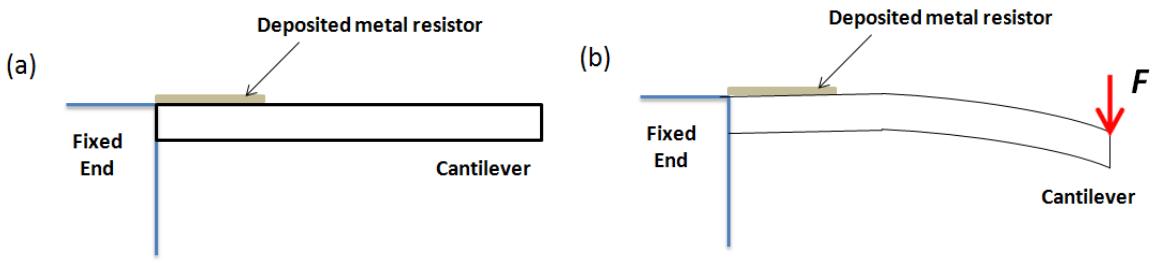

Figure 2.9 Schematic view of using thin metal film resistors for read-out

Figure 2.9a shows a cantilever with a thin metal film resistor deposited near the fixed end. When a transverse force is applied at the fixed end of the cantilever, the beam bends as shown in Figure2.9b, producing stress on the surface with the greatest magnitude presiding near the fixed end. The deposited metal resistor experiences tensile or compressing stress depending on the direction of the force. The stress changes the resistance value of the thin metal film resistor which can be detected.

2.4 Proposed design

SU-8 polymer is proposed as the device material as it is highly suitable for the fabrication of cantilever based sensors. The cantilevers are integrated with thin chromium film resistors for transduction. The schematic view of the proposed design of the polymer based cantilever is shown below in Figure 2.10.

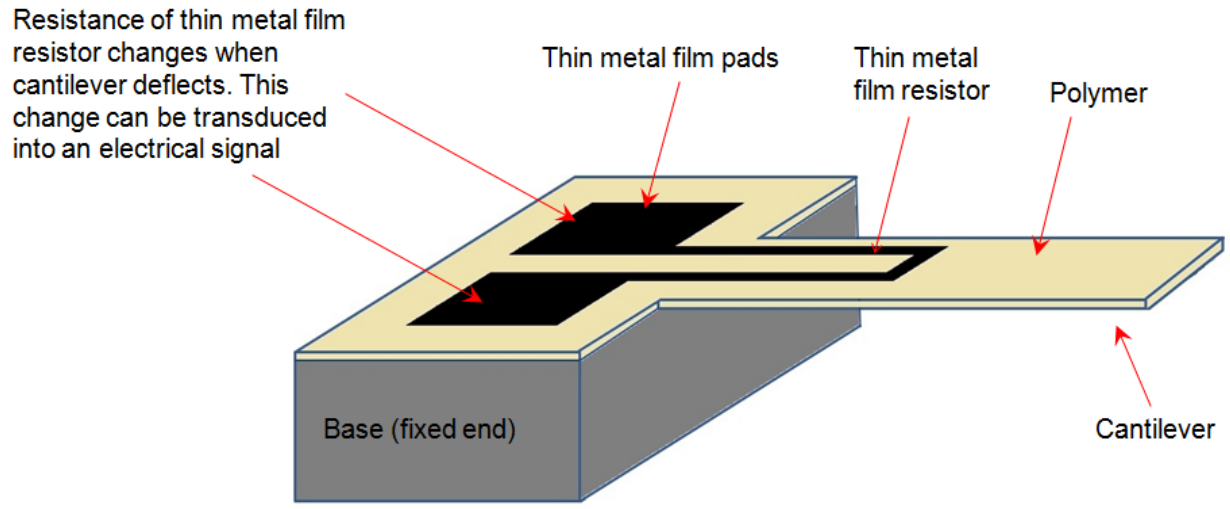

Figure 2.10 Schematic view of proposed design of polymer based cantilever

The cantilever is fabricated by SU-8 polymer. The cantilever is attached to a base which forms the fixed end. The base is an Aluminum sheet. A thin chromium film resistor is deposited

near the fixed end of the cantilever. When force is applied at the free end of the cantilever, the cantilever deflects inducing stress on the surface of the cantilever. The stress induced on the surface of the cantilever changes the resistance of the thin chromium film resistor. If an electrical contact is provided with the thin chromium film resistor, the change in resistance can be transduced into an electrical signal. This is achieved by fabricating thin chromium film pads where electrical contact with the help of thin wires can be made.

Chromium metal is proposed as the thin metal film resistor. It has high resistivity of 13 x 10^{-8} Ω.m. Chromium provides the highest resistance as thin films compared to other metals. It is easily fabricated by physical vapor deposition (PVD) techniques. It is inexpensive and readily available. The thin chromium film resistor controls the sensitivity of the cantilever. When a cantilever bends, the maximum strain is experienced on the fixed end. The maximum strain of the cantilever should not exceed the maximum strain of the thin chromium film resistor which is deposited on the surface of the cantilever near the fixed end otherwise the thin chromium film resistor will break making the cantilever based sensor non-functional. In section 2.1.3, the magnitude of the maximum strain produced by the cantilever on the fixed end was found out and is mentioned in Equation 29 which is as follows:

$$\varepsilon_{max} = [\ (6FL) / (Ewt^2)\ ] \qquad (29)$$

If maximum strain of thin chromium film resistor is known, the maximum force (F) that the cantilever can detect can be found out using Equation 29. After calculating the maximum assumed force a cantilever can withstand, the maximum deflection of the cantilever can be found out using Equation 24 which is as follows:

$$F = [\ (Ewt^3) / (4L^3)\ ].\ y_{max} \qquad (24)$$

Using the maximum strain value of chromium, the maximum assumed force and deflection of a cantilever can be known. To find out the maximum strain of thin chromium film resistor, Equation 3 can be used which is as follows:

$$E = \sigma / \varepsilon \quad (3)$$

The yield strength of PVD chromium can be considered as the maximum stress PVD chromium can withstand. Using the value of Young's modulus of PVD chromium, the maximum strain of PVD chromium can be found out. The Young's modulus and yield strength of PVD chromium are given as follows:

Young's modulus of PVD chromium = 140GPa ((Thin film) IEEE, MicroElectroMechanical Systems Workshop, Feb 1990, Napa Valley, California, p. 174)

Yield strength of PVD Chromium = 282MPa (Ultimate Tensile Strength (Recrystallized) Matweb)

Using Equation 3,

ε_{max} = (Yield strength of PVD chromium) / (Young's modulus of PVD chromium)

ε_{max} of PVD chromium = 282MPa / 140GPa = 2014.3 micro strain (assumed)

Using this value, the maximum force a cantilever can detect can be found out using Equation 29 and using the value of calculated maximum assumed force, the maximum deflection of a cantilever can be found out using Equation 24. In this way, the maximum strain of thin chromium film resistor controls the sensitivity of the cantilever.

Note that the physical dimensions of the cantilever i.e. L, w, t and Young's modulus of cantilever material (E) also play an important role in characterizing the sensitivity of the

cantilever along with the thin chromium film resistor. Changing the physical dimensions of the cantilever and the type of thin metal film resistor, the sensitivity of a cantilever can be controlled.

Chapter 3

Fabrication of polymer based micro scale force sensing cantilevers

The schematic illustration of the complete fabrication process flow of polymer based micro scale force sensing cantilevers is shown below in Figure 3.1.

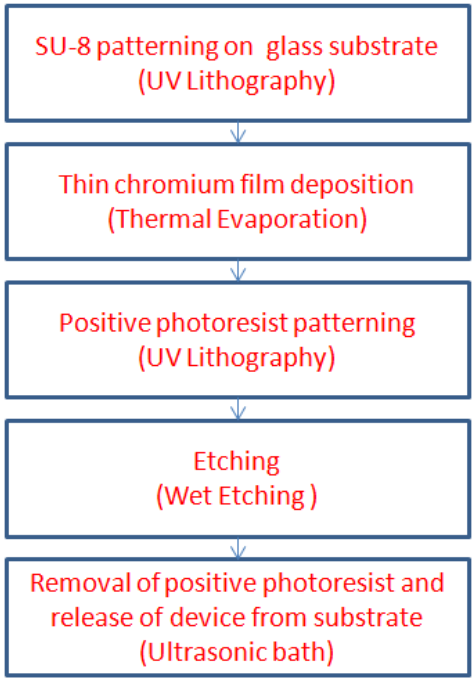

Figure 3.1 Schematic illustration of complete fabrication process flow

SU-8 negative photoresist polymer was patterned on a glass substrate followed by deposition of thin chromium metal film. To achieve a specific pattern of thin chromium film on SU-8, positive photoresist was patterned which acts as a masking layer. Wet etching was carried out to remove chromium metal which was not masked by the positive photoresist pattern. The positive photoresist pattern was resistant to the chromium etchant so the chromium film masked by positive photoresist remained. Then positive photoresist was removed and the device was released from the substrate using ultrasonic bath in acetone solution.

3.1 SU-8 patterning on glass substrate

The first step was the patterning of SU-8 on glass substrate. The patterning was achieved by UV lithography which is a process that uses UV light, a photomask and a photosensitive material (SU-8 2015, MicroChem USA) to facilitate the transfer of a specific pattern onto the substrate. A typical process flow of UV lithography to pattern SU-8 is shown below in Figure 3.2.

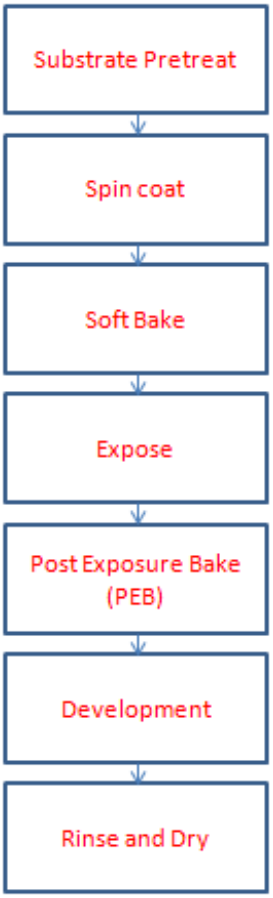

Figure 3.2 Typical process flow illustration of SU-8 patterning by UV lithography (Redrawn from MicroChem SU-8 processing guidelines)

3.1.1 Substrate pretreat

To obtain maximum process reliability, substrates should be clean and dry prior to applying SU-8 photoresist. Glass slides were used as substrates with dimensions 75mm x 35 mm. Each slide was cut into half to carry four cantilever devices. The glass slides were washed with Acetone prior to SU-8 spin coating and dried by spin coating itself.

3.1.2 Spin coating

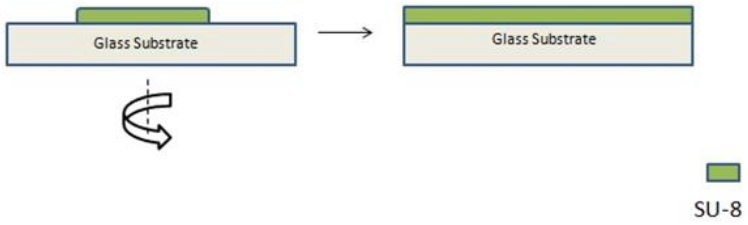

Figure 3.3 Side view schematic of spin coating SU-8 on glass substrate

The substrate was coated with a very thin layer of photo sensitive SU-8 negative photoresist by spin coating. The spin coater used was from Laurell Technologies Corporation, model: WS-650SZ-6NPP/LITE.

Program to spin coat 15µm SU-8 photoresist:

(Step1) Spin at 500 rpm for 10 seconds with acceleration of 100 rpm/second.

(Step2) Spin at 3000 rpm for 30 seconds with acceleration of 300 rpm/second.

Program to spin coat 17.5µm SU-8 photoresist:

(Step1) Spin at 500 rpm for 10 seconds with acceleration of 100 rpm/second.

(Step2) Spin at 2500 rpm for 30 seconds with acceleration of 300 rpm/second.

Spin coating was followed by soft baking performed at 97 degree Celsius for 3.5 minutes for SU-8 thickness of 17.5µm and 3 minutes for SU-8 thickness of 15µm. This drives away solvent from the deposited photoresist.

3.1.3 Exposure

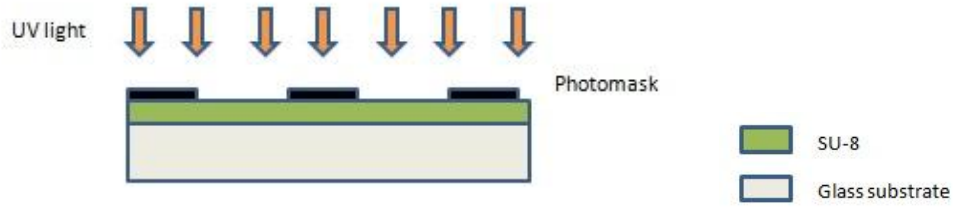

Figure 3.4 Schematic of UV light exposure

The SU-8 photoresist layer was exposed to a pattern of UV light defined by a photomask. The photomask was designed on L-Edit. It is shown below in Figure 3.5.

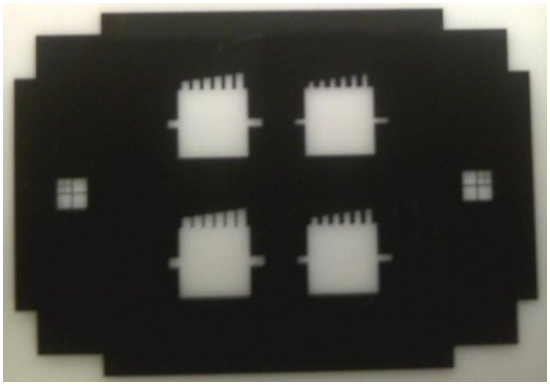

Figure 3.5 Photograph of photomask used to pattern SU-8 cantilevers

The pattern was aligned onto the substrate by a mask aligner. A mask aligner consists of a microscope and mechanical stages that facilitate precise alignment between the photomask and the substrate (Zhang and Hoshino, 2014). The exposure time of UV light was 8 seconds

calculated from the exposure power of the UV lamp machine which was 26.4mW / cm^2. The UV machine used was OAI Hybra Lign series 200IR. PEB was carried out just after exposure at 97 degree Celsius for 4.5 minutes for SU-8 thickness of 17.5µm and 4 minutes for SU-8 thickness of 15µm.

3.1.4 SU-8 development

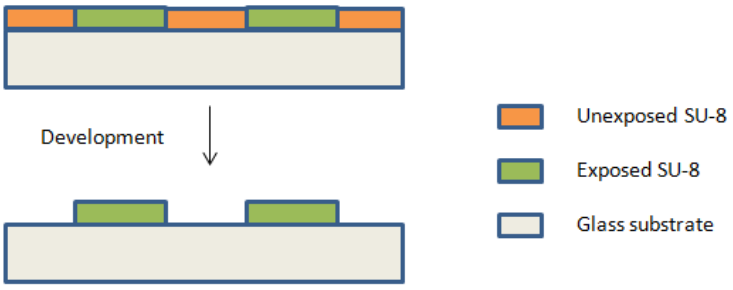

Figure 3.6 Schematic of SU-8 development

SU-8 photoresist is a negative photoresist. For a negative photoresist, the unexposed area is removed by the developing solution. The development was carried out for 3 minutes. The SU-8 developer (MicroChem, USA) was used for development. After development, the developed sample or image was washed with fresh solution for 10 seconds followed by a second wash with Isopropyl Alcohol (IPA) for 10 seconds. The sample was then dried. Figure 3.7 below shows microscopic images of SU-8 pattern on the substrate.

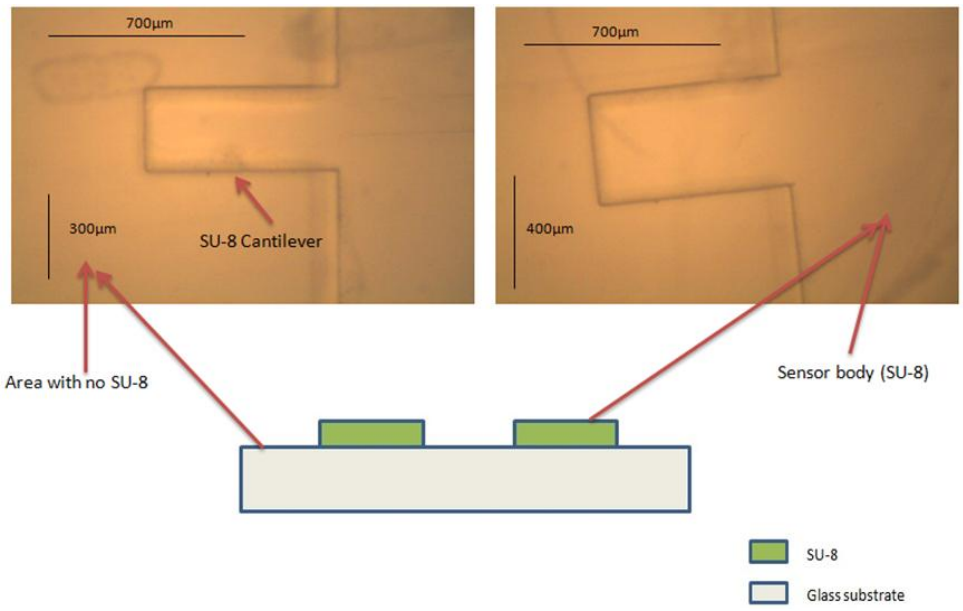

Figure 3.7 Microscopic images of SU-8 pattern on glass substrate

3.2 Thin chromium film deposition

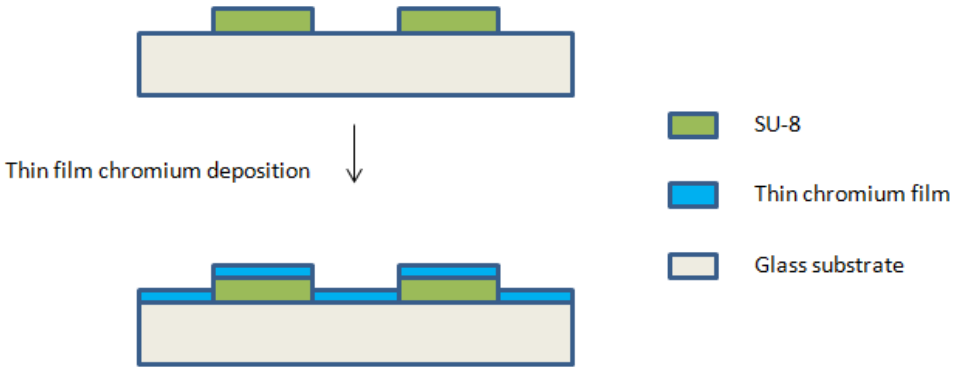

Figure 3.8 Schematic of thin chromium film deposition

After SU-8 patterning, the next step in the fabrication process was the deposition of thin chromium metal film. Before metal deposition, plasma treatment of the SU-8 pattern was carried out for about 35 seconds. Plasma Cleaner PDC-32G (Harrick Plasma) was used for plasma

treatment. Plasma treatment is believed to increase adhesion of polymers. Evaporation was used to deposit chromium metal as it is a process commonly used to deposit thin metal films. When the source (chromium metal pellets [Kurt J. Lesker]) was heated in a vacuum, it evaporated and released vapor particles, which travelled straight to the target substrate on which they were condensed back into a solid state (Zhang and Hoshino, 2014). Evaporation is a type of PVD. Resistive heat evaporation apparatus DV-502A (DENTON VACUUM) was used for metal deposition. It utilizes heat induced by current passing through a filament or a metal plate which holds the chromium pellets to be evaporated. A quartz crystal microbalance (QCM) based deposition monitor is commonly used with it. The QCM monitor (Maxtek, Inc) reading for chromium deposition was between 3.3 to 3.7 kÅ and the thickness of thin film of chromium was measured by dektak stylus profilometer (150 Veeco) which was found to be around ~ 50-70nm. Figure 3.9 below shows a microscopic image of the sample after metal deposition.

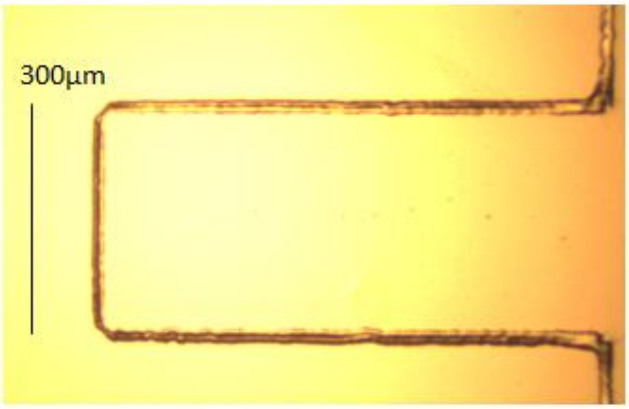

Figure 3.9 Microscopic image of SU-8 cantilever with thin chromium film on substrate

3.3 Positive photoresist patterning (masking layer)

The next step was the patterning of positive photoresist. The pattern was achieved by UV lithography with the process flow almost similar as patterning of SU-8. Microposit™ S1805™

positive photoresist (Rohm and Haas electronic materials) was used. The positive photoresist patterning was used to transfer the pattern on the thin chromium film. It acts as the masking layer. The process flow illustration for positive photoresist patterning by UV lithography is shown below in Figure 3.10.

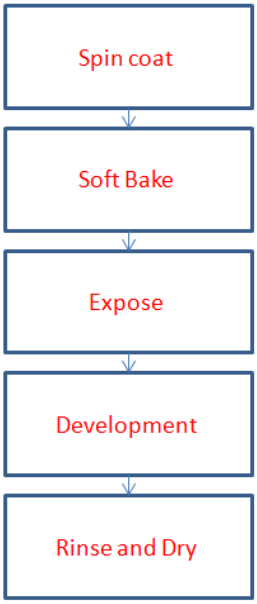

Figure 3.10 Schematic illustration for process flow of positive photoresist patterning

3.3.1 Spin coating

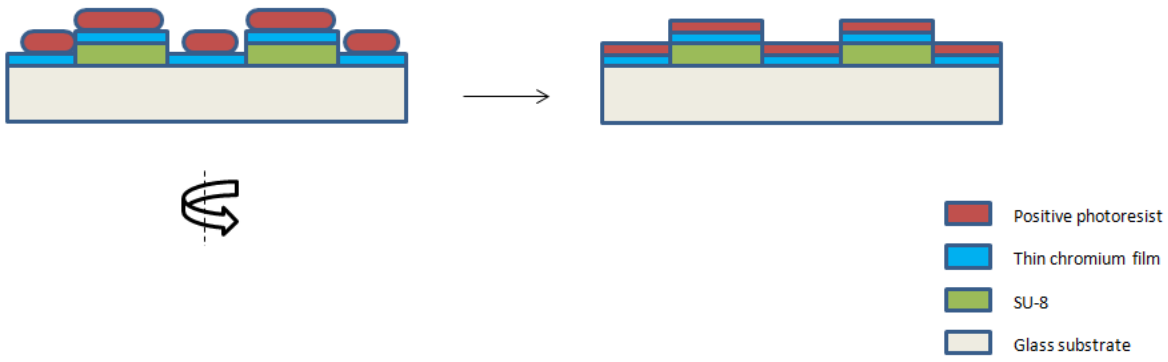

Figure 3.11 Schematic of positive photoresist spin coating

The SU-8 pattern on substrate coated with thin film of chromium was then spin coated with positive photoresist using the spin coater.

Program to spin coat positive photoresist:

(Step1) Spin at 500 rpm for 5 seconds with acceleration of 500 rpm/second.

(Step2) Spin at 1500 rpm for 45 seconds with acceleration of 1000 rpm/second.

Spin coating of positive photoresist was followed by soft baking performed at 113 degree Celsius for 1.5 minutes. The thickness of positive photoresist was ~600nm (Dektak stylus profilometer).

3.3.2 Exposure

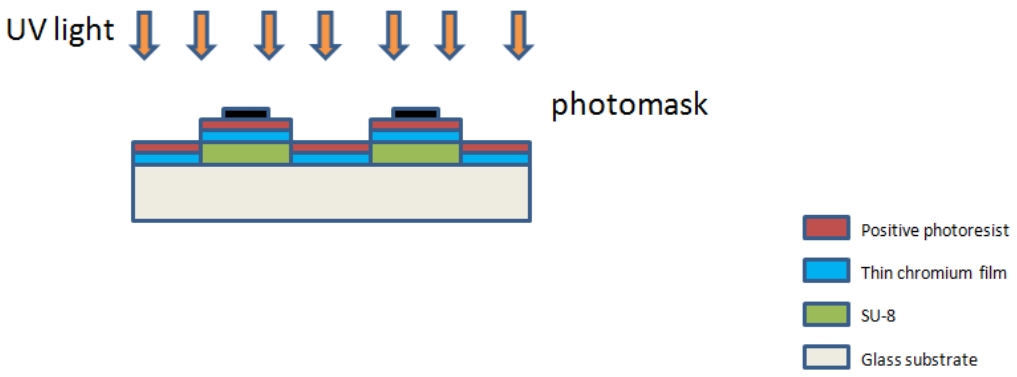

Figure 3.12 Schematic of UV light exposure

The SU-8 pattern coated with thin chromium film was exposed to a pattern of UV light defined by another photomask. The photomask of this pattern was also designed on L-Edit. It is shown below in Figure 3.13.

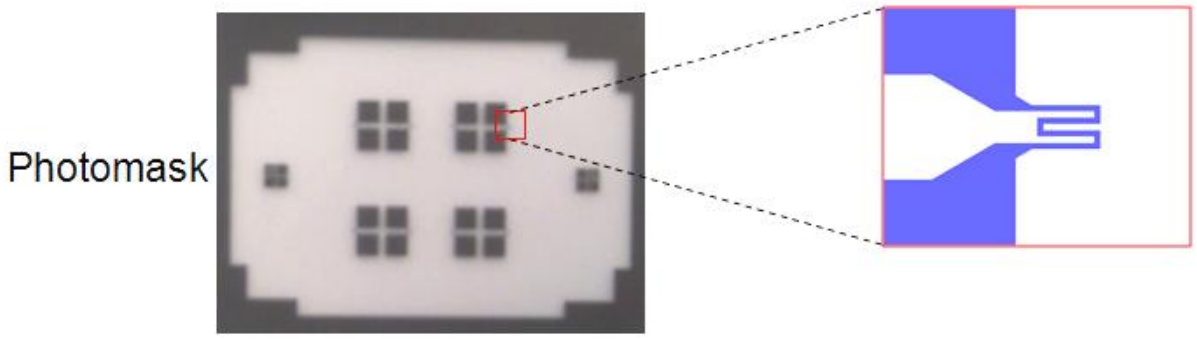

Figure 3.13 Photograph of photomask used to pattern positive photoresist

The photomask consists of alignment marks which were also present on the previous photomask used to pattern SU-8. This helped to precisely align the thin metal film pads and thin metal film resistor patterns on this photomask to the SU-8 which was already patterned. The exposure time of UV light was 4 seconds. The selected area in above figure on the right side is the magnified image of the thin chromium film resistor pattern deposited on the surface of the cantilever near the fixed end. The length of the thin chromium film resistor was 1290µm.

3.3.3 Positive photoresist development

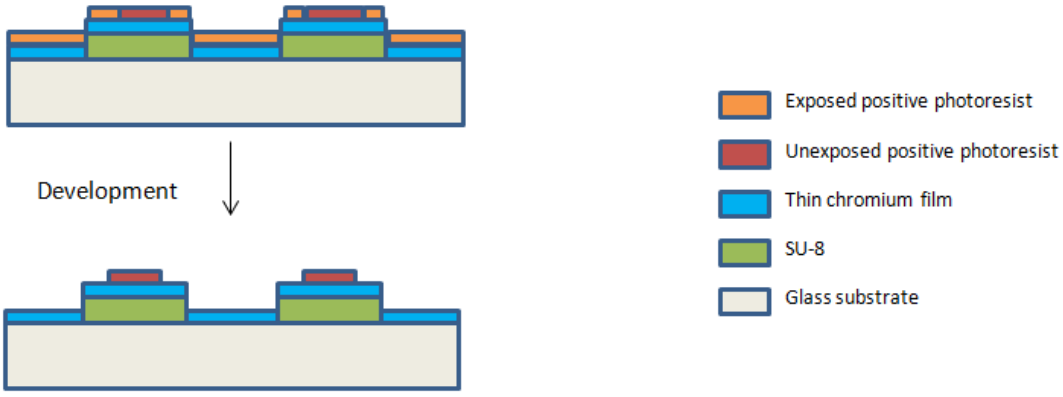

Figure 3.14 Schematic of positive photoresist development

S1805^{TM} is a positive photoresist. For a positive photoresist, the exposed part was removed by the developing solution. After development, only the unexposed part of positive photoresist remains on the thin chromium film. This unexposed pattern of the positive photoresist was the pattern of thin chromium film resistor and thin chromium film pads. AZ 300 MIF Developer (AZ Electronic Materials) was used as the developing solution. The development was carried out for 12 seconds. After development, the sample was rinsed with distilled water and then dried. Figure 3.15 below shows microscopic image obtained after positive photoresist patterning.

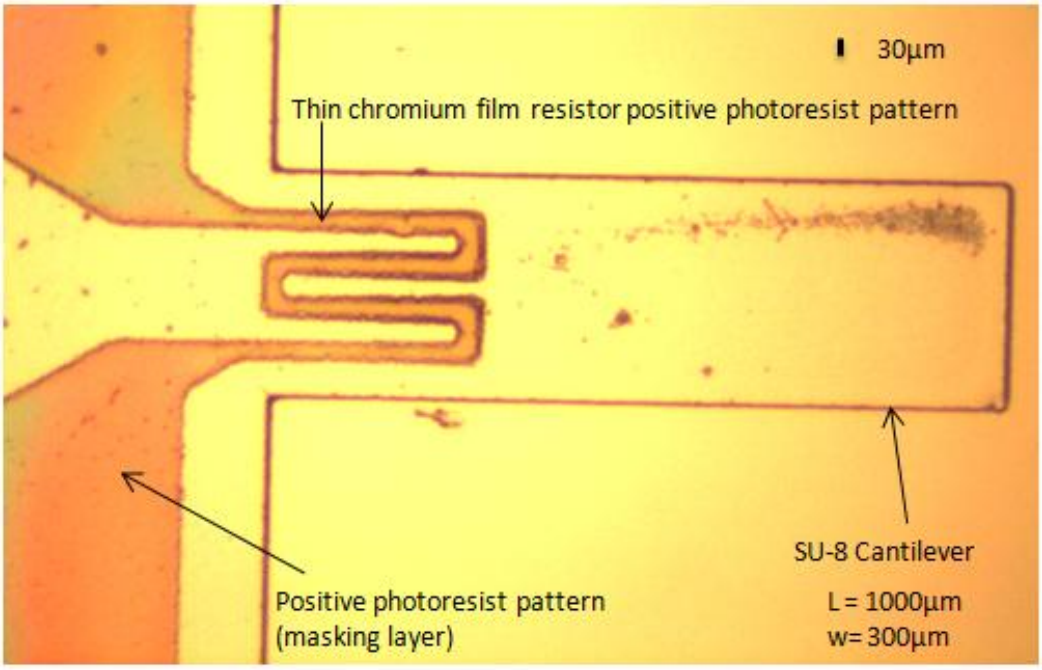

Figure 3.15 Microscopic image of SU-8 cantilever coated with thin chromium film and positive photoresist pattern. The substrate is coated with SU-8 pattern, thin chromium film and positive photoresist pattern

3.4 Etching

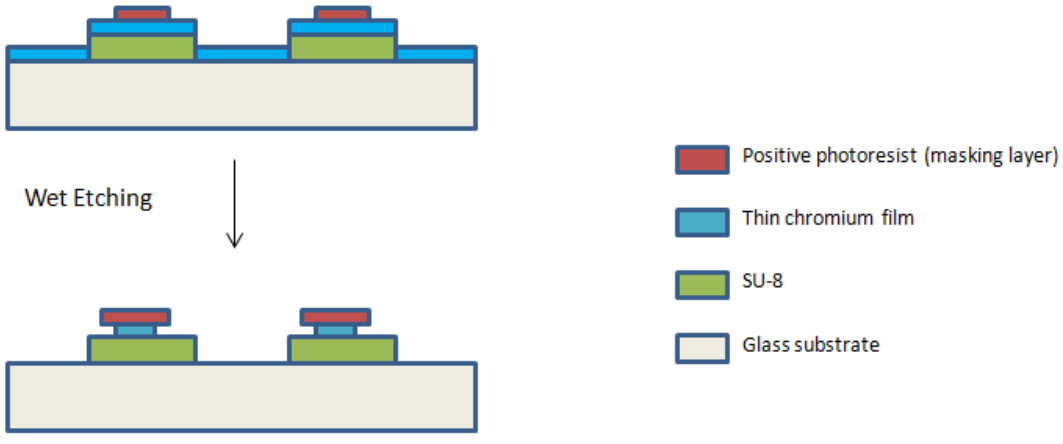

Figure 3.16 Schematic of wet etching

After positive photoresist patterning, the next step in the fabrication process was etching. Etching is a process that translates a two dimensional pattern onto a structural layer underneath the top masking layer (Zhang and Hoshino, 2014). The positive photoresist pattern acts as the masking mask. Wet etching uses a chemical solution or an etchant to cut or etch metals. Chromium Etchant 1020 (Transene Company, Inc) was used to etch the thin chromium film. The thin chromium film resistor pattern needed on the SU-8 pattern was masked by a photoresist pattern. The thin chromium film resistor and thin chromium film pads are the target patterns on the SU-8 pattern that's why the masking layer which is the positive photoresist pattern has the same pattern. When the sample is immersed in the etchant, the thin chromium film masked by the positive photoresist pattern remains while the rest chromium film is removed or etched. The positive photoresist is resistant to the etchant. Before etching the sample, plasma treatment was carried out for 35 seconds followed by hard baking performed at 150 degree Celsius for 5 minutes. Hard Bake makes the positive photoresist pattern more resistant to the etchant which helps to mask the thin chromium film to be patterned on SU-8. Then the sample was immersed in

the chromium etchant solution until the chromium film not masked by positive photoresist was removed.

3.5 Removal of positive photoresist and release of device from substrate

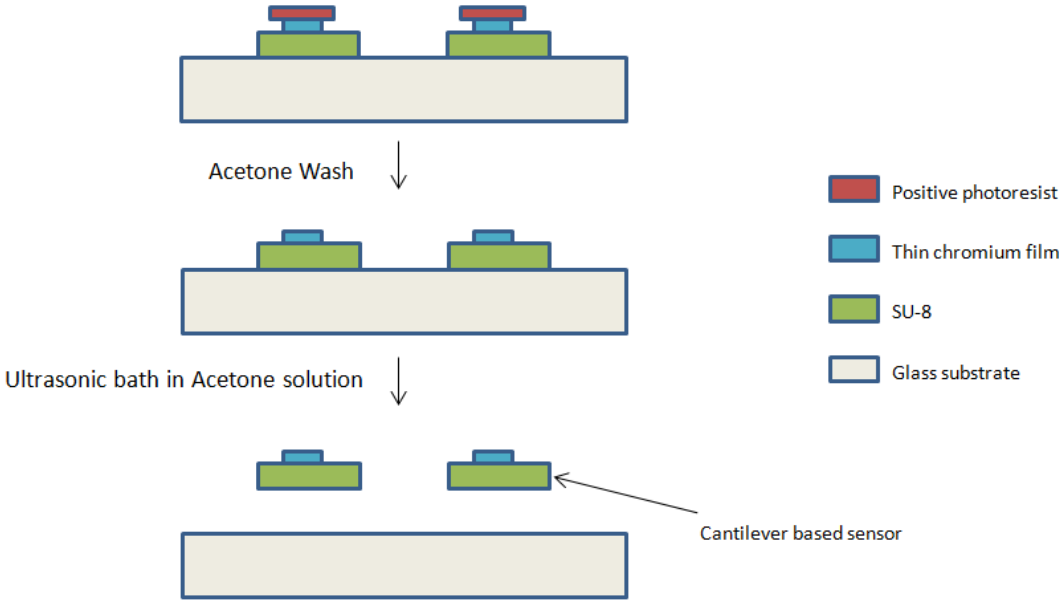

Figure 3.17 Schematic of removal of positive photoresist and release of device from substrate

After etching, the sample was immersed in Acetone solution and an ultrasonic bath was performed. This helped to remove the positive photoresist pattern and the cantilever based sensors came off from the substrate. The sensors were collected and dried. Figure 3.18 below shows microscopic images of the cantilever based sensor.

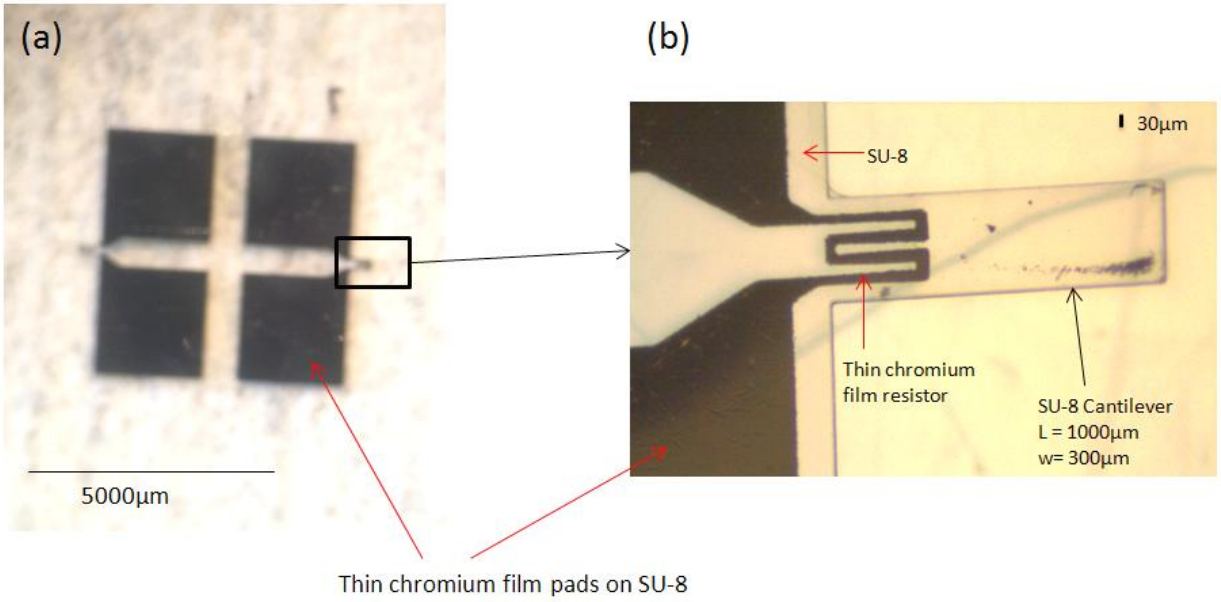

Figure3.18 (a) Microscopic image of polymer based cantilever integrated with thin chromium film resistor (b) Magnified image of cantilever

Chapter 4

Experimental setup, results and analysis

Cantilevers with different physical dimensions were fabricated. The width of the cantilevers ranged from 300µm to 600µm, the thickness was chosen to be 15µm and 17.5µm and the length of the cantilevers was chosen to be 700µm and 1000µm. This provides a variety of cantilevers with different stiffness values and a wide range of force can be detected. These dimensions were chosen because the stiffness values of cantilevers coincide with the stiffness values of cantilevers being used in studies for micro scale testing. Another reason is that it is easy to fabricate cantilevers with these dimensions. Using these cantilevers, set of experiments were carried out. In this chapter, the experiments, experimental setup, results from experiments and related discussion is explained. After fabricating cantilever based sensors, the experimental setup was prepared.

4.1 Preparation of experimental setup

In order to perform experiments, fabricated cantilever based sensors were attached to a base. The sensors were attached to an Aluminum sheet. Then electrical wires were glued on the thin chromium film pads.

4.1.1 Attachment of cantilever based sensor on a base

In order to move the cantilever based sensor smoothly, it is important to hold the cantilever and attach it with a base. The cantilever based sensor was glued on an Aluminum sheet that was cut and shaped with respect to the design of the sensor. Figure 4.1 below shows the attachment.

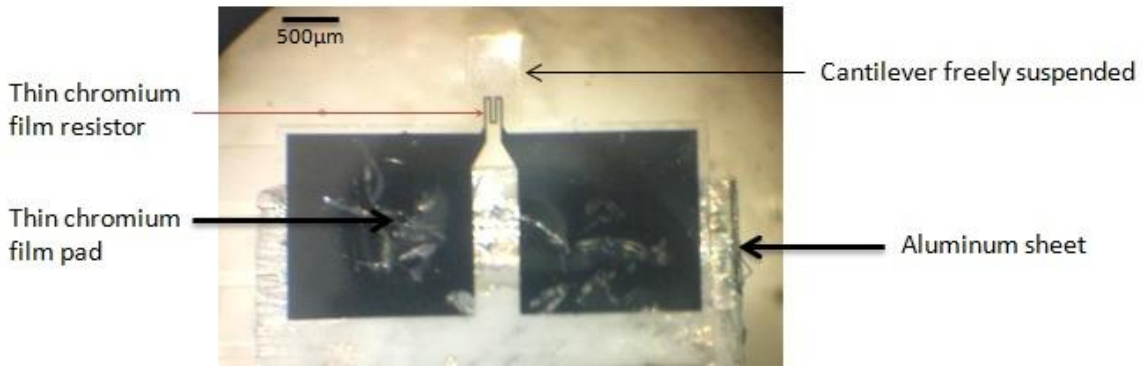

Figure 4.1 Cantilever based sensor attached to Aluminum sheet

4.1.2 Electrical connection of wires with thin chromium film pads for transduction

After attachment of the sensor with Aluminum sheet, thin electrical wires were connected with the thin chromium film pads. The wires should be placed on to the thin chromium film pads such that they don't move and have a good contact with the pad surface. For this purpose very thin wires were placed in such a way that near the contact, the wires were bent. Figure 4.2 below shows the arrangement.

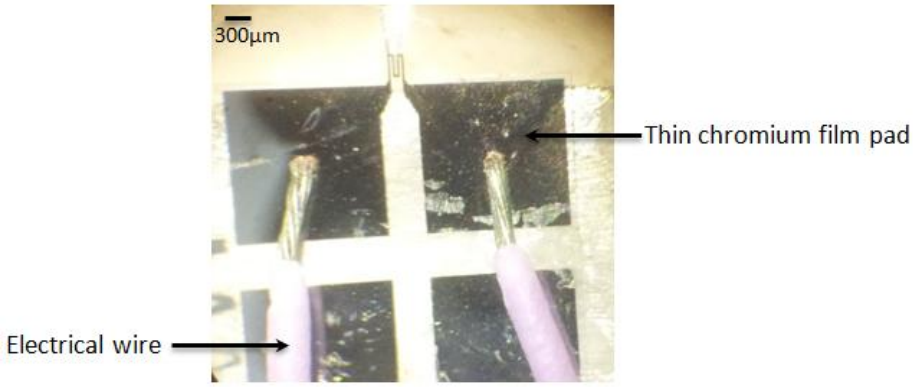

Figure 4.2 Placement of electrical wires on thin chromium film pads

After placing the wires, the electrical contact was made stable by using silver epoxy glue on the contact area. To cure the epoxy glue, the aluminum sheet carrying the sensor was placed

on a hot plate for 2.5 hours at 125 degree Celsius. To check whether the silver epoxy glue is cured, the resistance at the end of the wires should be almost the same as the resistance measured between the thin chromium film pads before attaching the sensor. Figure 4.3 below shows a microscopic image after the wires were connected with the thin chromium film pads on the sensor and the silver epoxy glue was cured.

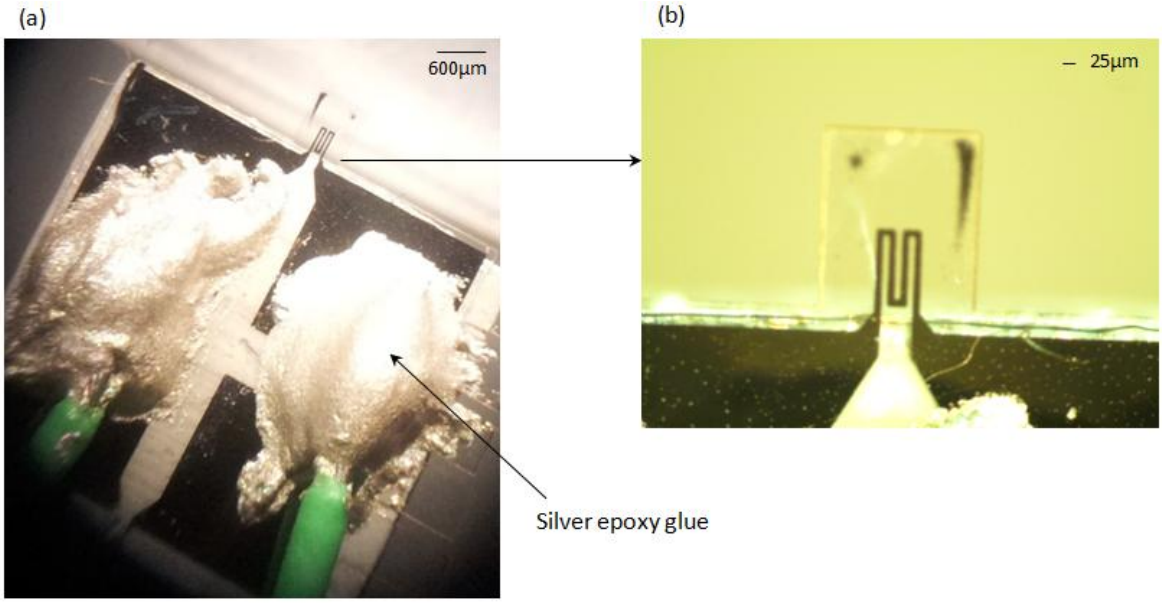

Figure 4.3 (a) Microscopic image of electrical wires connected to thin chromium film pads of the cantilever based sensor. (b) Magnified image of the cantilever

Before attaching the cantilever based sensor to the base, the resistance of the thin chromium film resistor was measured using a digital multi-meter. The electrodes of the digital multi-meter were placed directly on the two thin chromium film pads which form extreme ends of the thin chromium film resistor. After attaching the sensor to the Aluminum sheet and gluing electrical wires on the thin chromium film pads, the resistance was measured between the two electrical wires. This resistance should be almost the same resistance that was measured directly between the thin chromium film pads. This ensures the silver epoxy glue is cured.

4.2 Experimental setup

Figure 4.4 below shows the photograph of the experimental setup used to carry out the experiments.

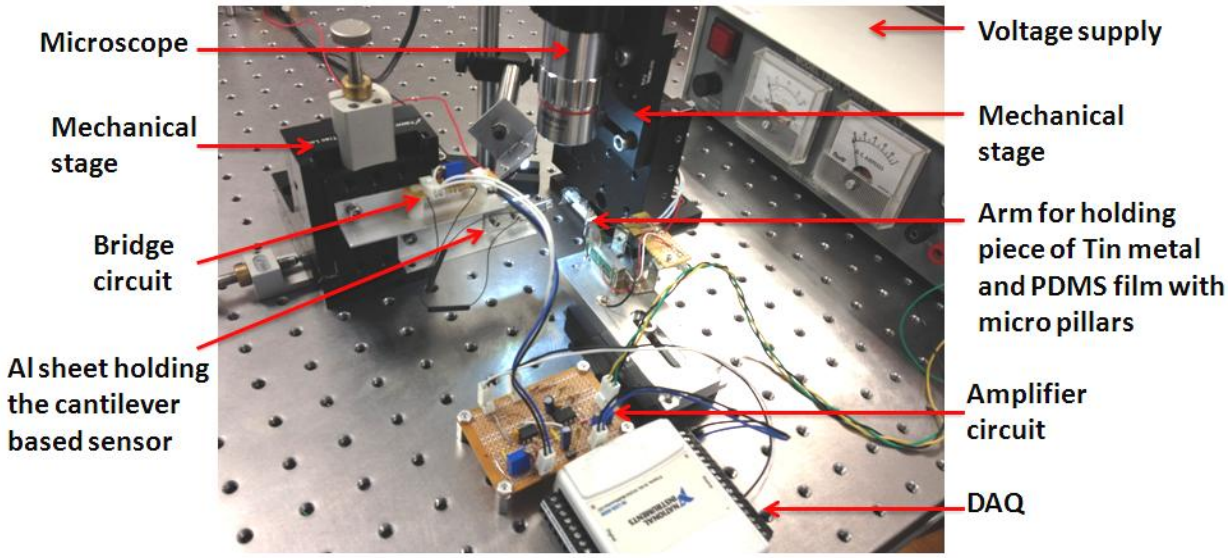

Figure 4.4 Photograph of experimental setup

The cantilever based sensor was attached to an Aluminum sheet. This Aluminum sheet was attached to another Aluminum sheet which was tilted and connected to a mechanical stage so that the movement of the cantilever could be made possible by the movement of the mechanical stage. An optical microscope was attached to another mechanical stage which only moves in upward and downward direction to focus the image. As the Aluminum sheet was tilted and connected to the mechanical stage, the side view of the cantilever would be imaged. An arm was also focused under the microscope. This arm holds the target material against which the cantilevers were moved. The arm was still throughout all the experiments. A piece of tin metal was used for the calibration of the cantilevers. To find the stiffness of elastic PDMS micro pillar, a film with PDMS micro pillars was held by the arm. To measure force in cancer cell

manipulation, centrifuged cancer cells were pasted on a PDMS film designed to hold the cells and this film was held by the arm. The top view of the arm holding target material would be imaged under the microscope.

The wires that have electrical connection with the thin chromium film resistor on the cantilever were connected to a bridge circuit. These wires provide resistance. The schematic view of the bridge circuit is shown below in Figure 4.5.

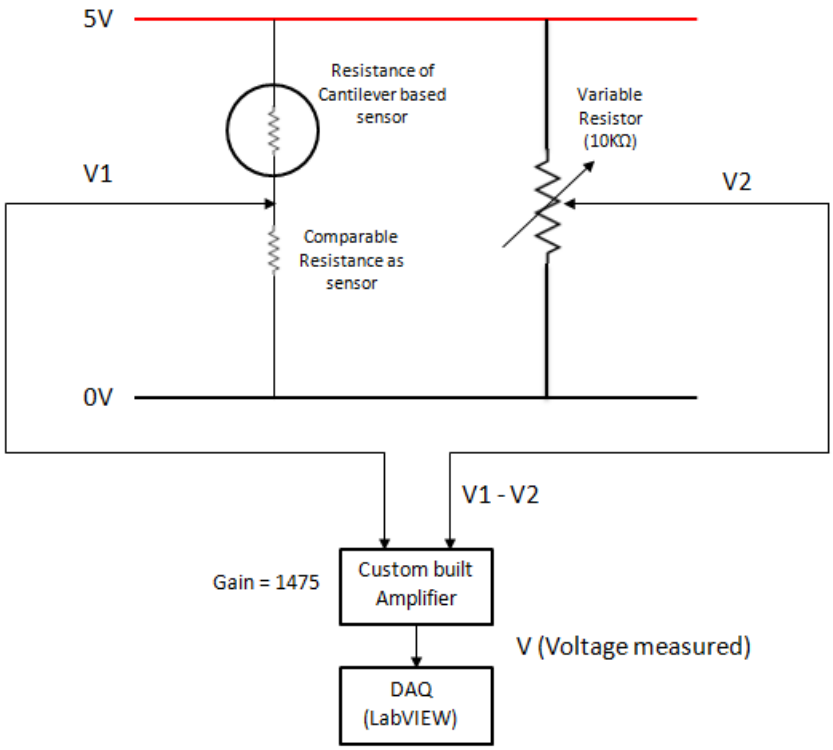

Figure 4.5 Schematic view of the bridge circuit

The wires connected to the thin chromium film resistor provide resistance of the cantilever based sensor. One of the wires was connected to 5V while the other wire was connected in series with a resistor of comparable value as the sensor, which was grounded. In parallel, a variable resistor of 10 KΩ was connected. In between the resistance provided by the

cantilever based sensor and the comparable resistor, a connection was made to get the Voltage (V1). Another connection was taken from the variable resistor to get Voltage (V2). V1 and V2 should be 2.5V each. These connections form the input of a custom built amplifier such that the difference Voltage (V1-V2) is amplified by a gain of 1475. The gain and offset of the amplifier can be adjusted. The arrangement is such that when the cantilever doesn't deflect the resistance of the cantilever based sensor doesn't change and the difference Voltage is zero. When the cantilever deflects, V1 changes, changing the difference Voltage (V1-V2) which is amplified by the custom built amplifier. The difference Voltage (V1-V2) is positive or negative depending on the direction of cantilever deflection. The output of the amplifier was connected to a USB Data Acquisition (National Instruments). The USB provides interface to a PC. Using LabVIEW, the amplified Voltage was measured and displayed. A voltage supplier was used to provide 15V to the custom built amplifier. A LED light was also used to achieve bright clear microscopic images.

4.3 Experiment to calibrate cantilevers

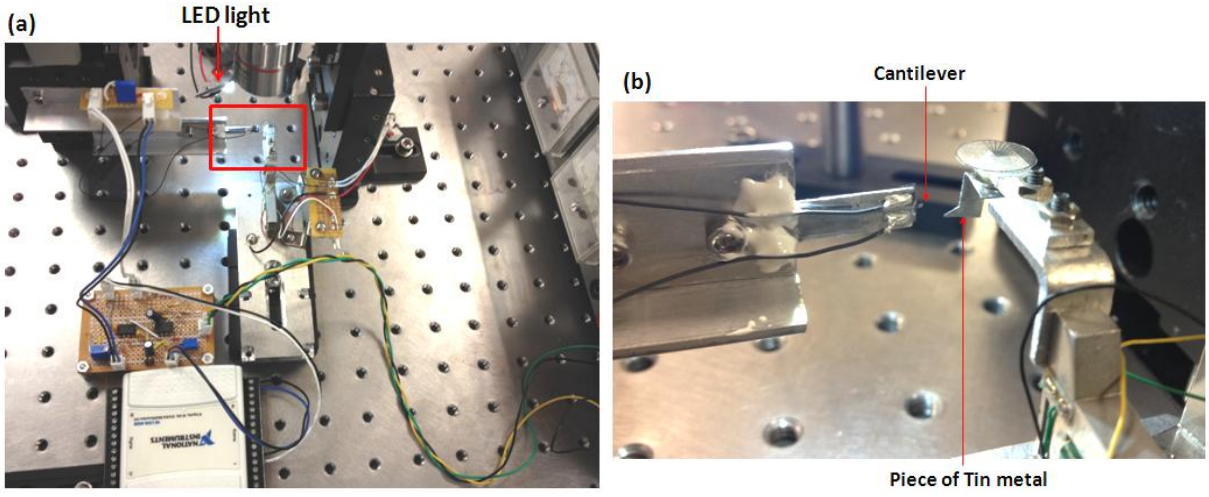

Figure 4.6 (a) Top view of experimental setup (b) Magnified image of selected area in (a)

The experimental setup to calibrate cantilevers is shown above in Figure 4.6. A piece of tin metal attached to the arm was used to calibrate the cantilevers. Figure 4.6 (a) shows the top view of the experimental setup and Figure 4.6 (b) shows the cantilever based sensor attached to the Aluminum sheet. The optical microscope imaged the top view of the arm and side view of the cantilever. The arm holding the tin metal piece was still throughout all experiments and focused under the microscope. The mechanical stage was used for the movement of the cantilever. With the help of the mechanical stage the cantilever was brought close to the piece of tin metal. This is shown below in Figure 4.7.

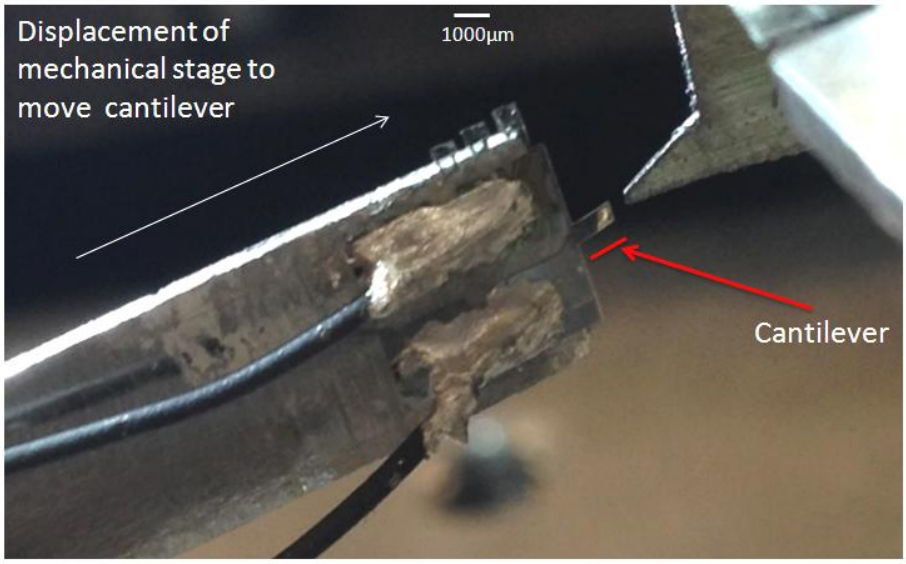

Figure 4.7 Image of cantilever based sensor movement towards the piece of tin metal

After the cantilever was brought close to the piece of tin metal, the mechanical stage was displaced in such a way that the free end of the cantilever touched the tin metal piece at one side. Then the mechanical stage was displaced in a direction towards the other side shown in Figure 4.8 such that the cantilever deflected. The deflection of the cantilever changed the voltage which was measured using LabVIEW.

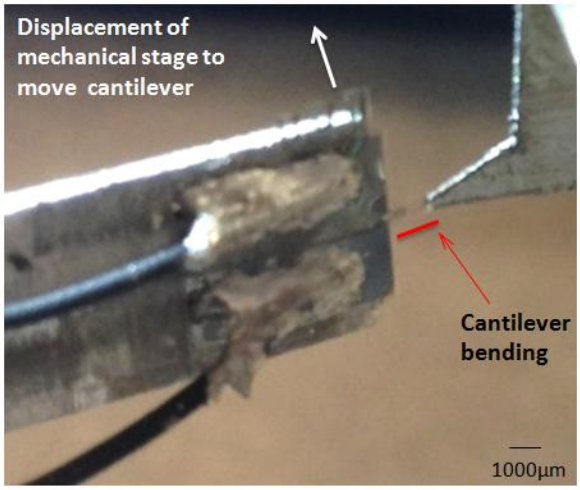

Figure 4.8 Image of cantilever deflecting when it is moved against tin metal

Before the experiment, some characters were assigned to represent specific measurements and calculations.

S = Spring constant of cantilever beam (stiffness of cantilever). It is calculated from the following relation and is a theoretical value

$$S = Ewt^3 / 4L^3 \qquad (30)$$

Where,

E = Young's modulus of SU-8 = 2.2GPa

w = width of cantilever

t = thickness of cantilever

L = length of cantilever

D = Displacement of mechanical stage to move the cantilever (upward direction +*D* and downward direction -*D*). It is measured from optical microscope.

δ = Deflection of the cantilever at free end. It is measured from optical microscope.

F = Force experienced at the free end of the cantilever when the cantilever bends. It is calculated from the measured deflection as follows and is an assumed value.

$$F = S \cdot \delta \qquad (24)$$

V = the difference voltage from the bridge circuit is amplified with a gain of 1475. V is the amplified voltage measured in LabVIEW.

ΔV = same voltage as in LabVIEW but without offset.

Figure 4.9 below shows the microscopic images of the experiment to calibrate cantilevers. As mentioned before, the microscope was mounted on the top which views the top view of the arm holding the tin metal piece and side view of the cantilever. As shown in Figure 4.9a, the cantilever was brought close such that the free end touches the tin metal. Then the mechanical stage was displaced in $-D$ direction with a small displacement causing the cantilever to deflect. As tin metal is very stiff, $\boldsymbol{D = \delta}$**.** The deflection causes a change in voltage which was measured. Then the mechanical stage was displaced further with a small displacement and the deflection and voltage was measured. The mechanical stage was displaced until the cantilever reaches a deflection shown in Figure 4.9b. F experienced at the free end of the cantilever causes the deflection. In this way, the cantilever was calibrated in $-D$ direction.

The cantilever was calibrated in $+D$ direction in a similar way as shown in Figure 4.9c. The cantilever was brought close to the tin metal but on the other side until the free end touches the tin metal. Then the mechanical stage was displaced in $+D$ direction causing the cantilever to deflect to the opposite side. This deflection changes the voltage which was measured. The mechanical stage was displaced until the cantilever reaches a deflection shown in Figure 4.9d.

F experienced at the free end of the cantilever causes the deflection. In this way, cantilevers with different stiffness values and physical dimensions were calibrated.

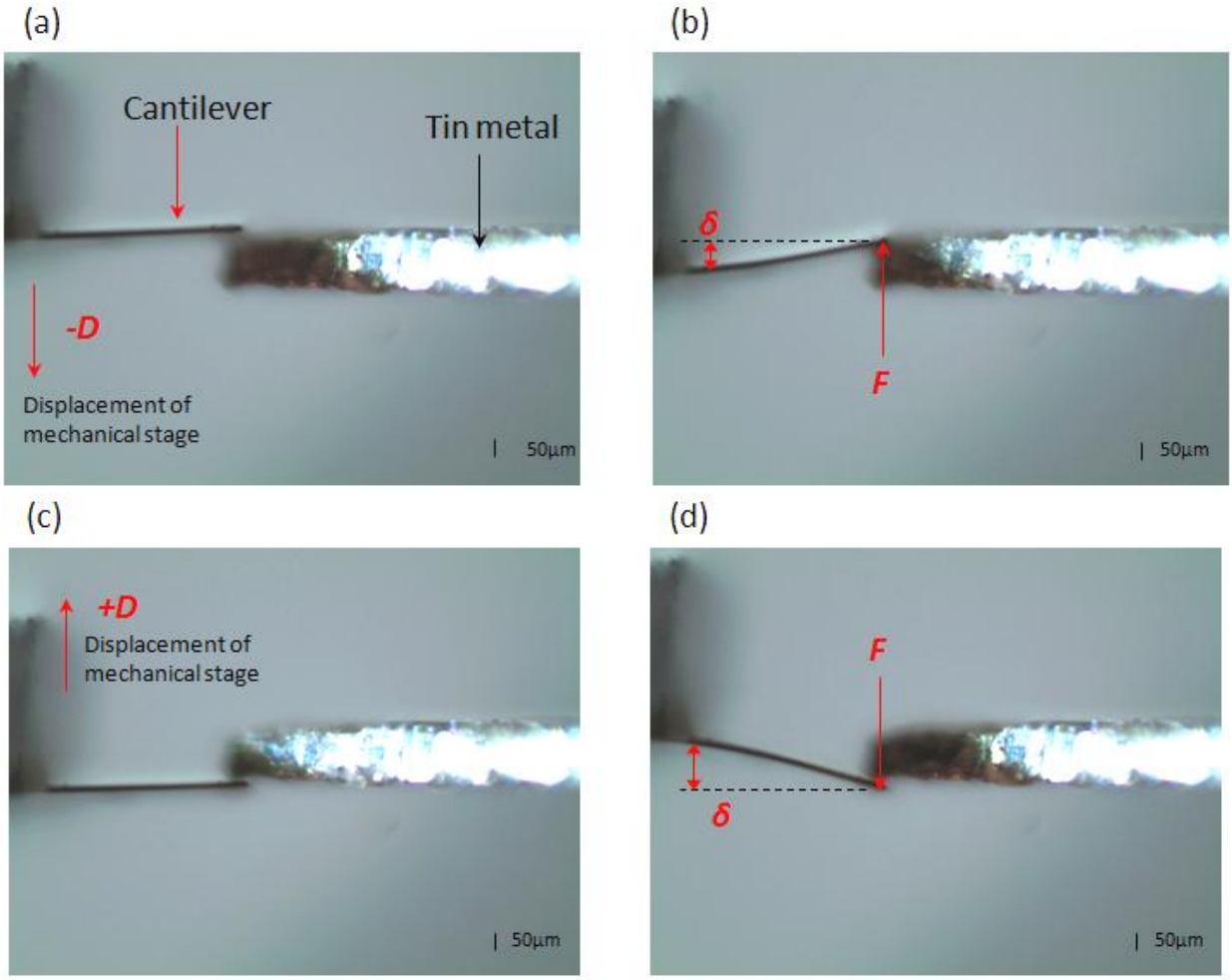

Figure 4.9 Microscopic images of cantilever calibration

4.3.1 Results

Four cantilevers with different stiffness values and physical dimensions were calibrated in both *–D* and *+D* directions carrying out the experiment shown in Figure 4.9 above. The stiffness of each cantilever was calculated by using the relationship as follows

$$S = Ewt^3 / 4L^3 \qquad (30)$$

The resistance (R) of the thin chromium film resistor of each cantilever was measured by a digital multi-meter. The deflection (δ) was measured using optical microscope. Force (*F*) was calculated from the measured δ using the relationship *F*=S.δ. As mentioned in Chapter 2, using the maximum strain value of PVD chromium i.e. 2014.3 micro strain, the maximum *F* that the cantilever can withstand was calculated for each cantilever using Equation (29) as follows. This is a theoretical value.

$$\varepsilon_{max} = 6FL / Ewt^2 \qquad (29)$$

From this theoretical F_{max}, using Equation (24) as follows, the maximum theoretical δ for each cantilever was calculated.

$$F_{max} = (Ewt^3 / 4L^3).\delta_{max} \qquad (24)$$

For each cantilever, ΔV measured from LabVIEW when the cantilever deflected was plotted against deflection (δ) of the cantilever and force (*F*) experienced at the free end of the cantilever. The cantilever with stiffness 5.156 Nm^{-1} was calibrated in both directions and is shown below in Figure 4.10.

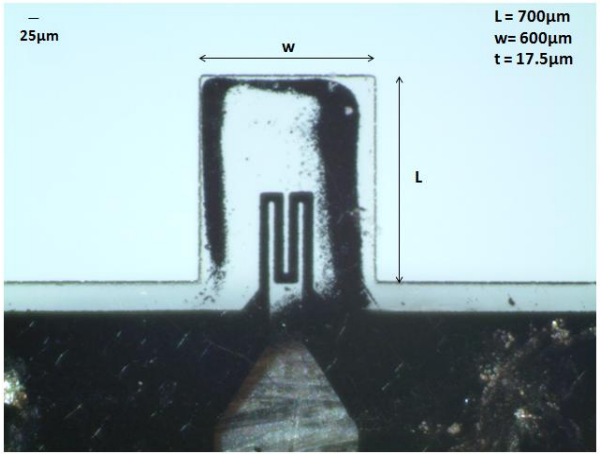

Figure 4.10 Microscopic image of cantilever with stiffness 5.156 Nm^{-1}

The measurements and calculations were recorded and are shown below in Table 4.1. The ΔV vs. δ and *F* vs. ΔV plots of the cantilever calibration in *–D* direction are shown in Figure 4.11 a and b respectively and in *+D* direction are shown in Figure 4.11 c and d.

Table 4.1 Measurements and calculations of cantilever having stiffness 5.156 Nm^{-1}

R measured 6.52 KΩ	F_{max} (Theoretical) 194µN	*F* calculated from measured δ 536µN
Stiffness (Theoretical) 5.156 Nm^{-1}	δ_{max} (Theoretical) 37.6µm	δ measured 104µm

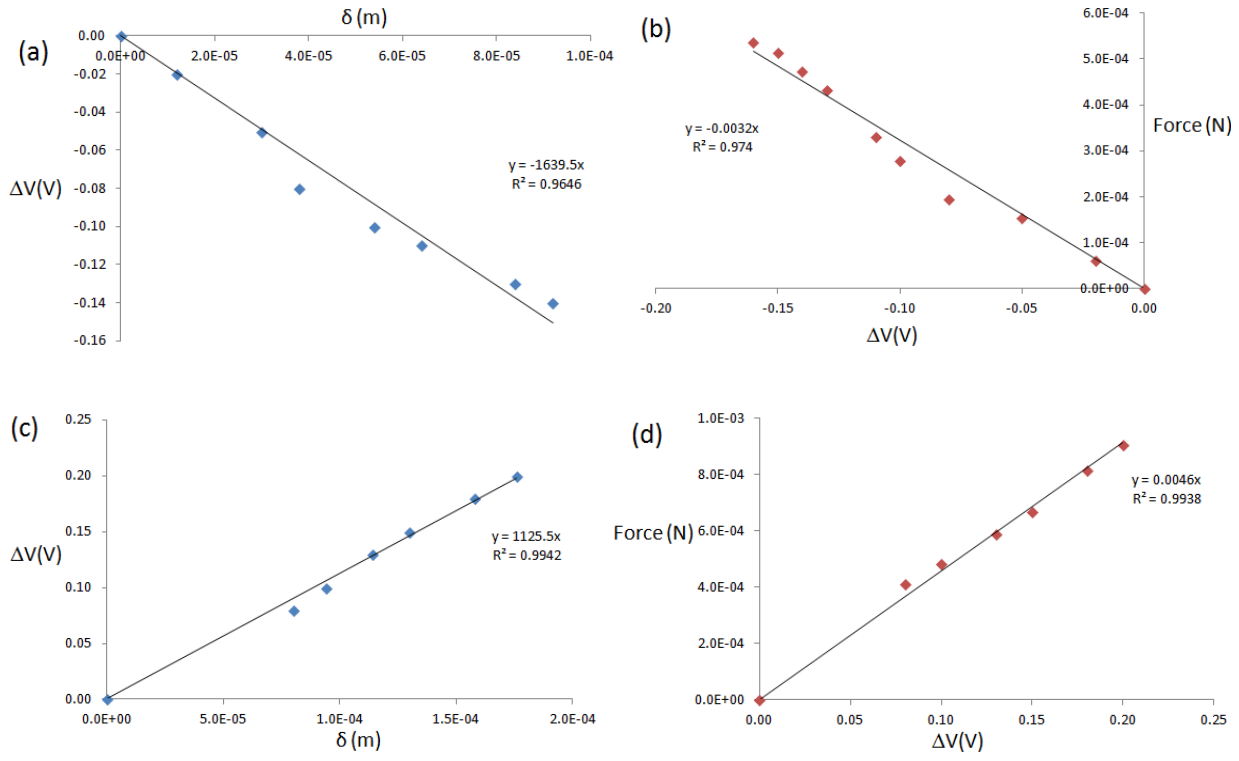

Figure 4.11 Results of sensor calibration. (a) ΔV vs. δ plot in *-D* direction (b) F vs. ΔV plot in *-D* direction (c) ΔV vs. δ plot in *+D* direction (d) F vs. ΔV plot in *+D* direction

The cantilever with stiffness 0.557 Nm^{-1} was also calibrated and is shown below in Figure 4.12. The measurements and calculations are shown in Table 4.2 and plots of sensor calibration are shown in Figure 4.13.

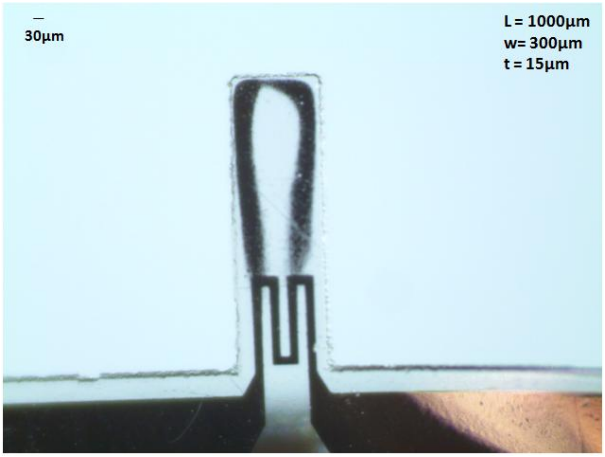

Figure 4.12 Microscopic image of cantilever with stiffness 0.557Nm^{-1}

Table 4.2 Measurements and calculations of cantilever having stiffness 0.557 Nm^{-1}

R measured 11.96 KΩ	F_{max} (Theoretical) 49.8µN	F calculated from measured δ 94.7µN
Stiffness (Theoretical) 0.557 Nm^{-1}	δ_{max} (Theoretical) 89.5µm	δ measured 170µm

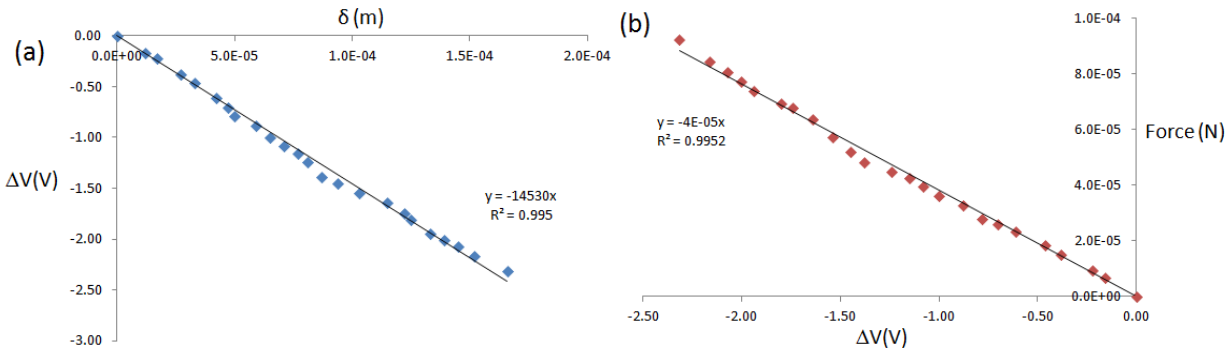

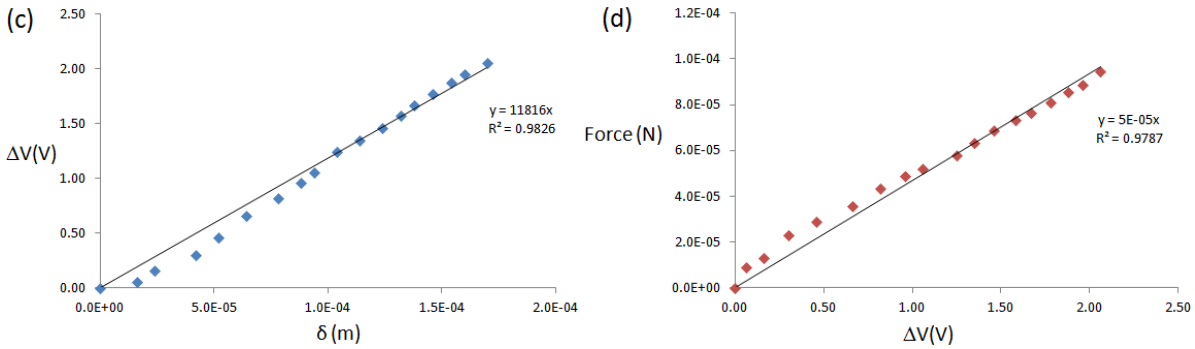

Figure 4.13 Results of sensor calibration. (a) ΔV vs. δ plot in -*D* direction (b) F vs. ΔV plot in -*D* direction (c) ΔV vs. δ plot in +*D* direction (d) F vs. ΔV plot in +*D* direction

Another cantilever with stiffness 0.928 Nm^{-1} was calibrated and is shown in Figure 4.14. The measurements and calculations are shown in Table 4.3 and plots of sensor calibration are shown in Figure 4.15.

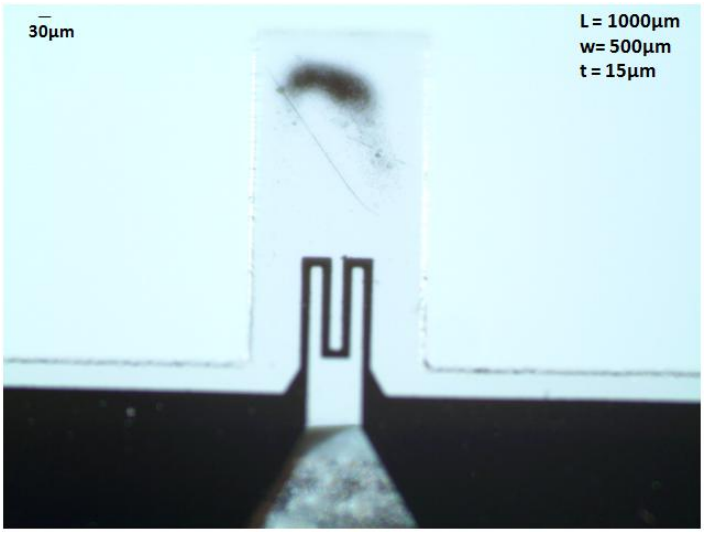

Figure 4.14 Microscopic image of cantilever with stiffness 0.928 Nm^{-1}

Table 4.3 Measurements and calculations of cantilever having stiffness 0.928 Nm^{-1}

R measured 7.72 KΩ	F_{max} (Theoretical) 83.1µN	*F* calculated from measured δ 159µN
Stiffness (Theoretical) 0.928 Nm^{-1}	δ_{max} (Theoretical) 89.5µm	δ measured 171µm

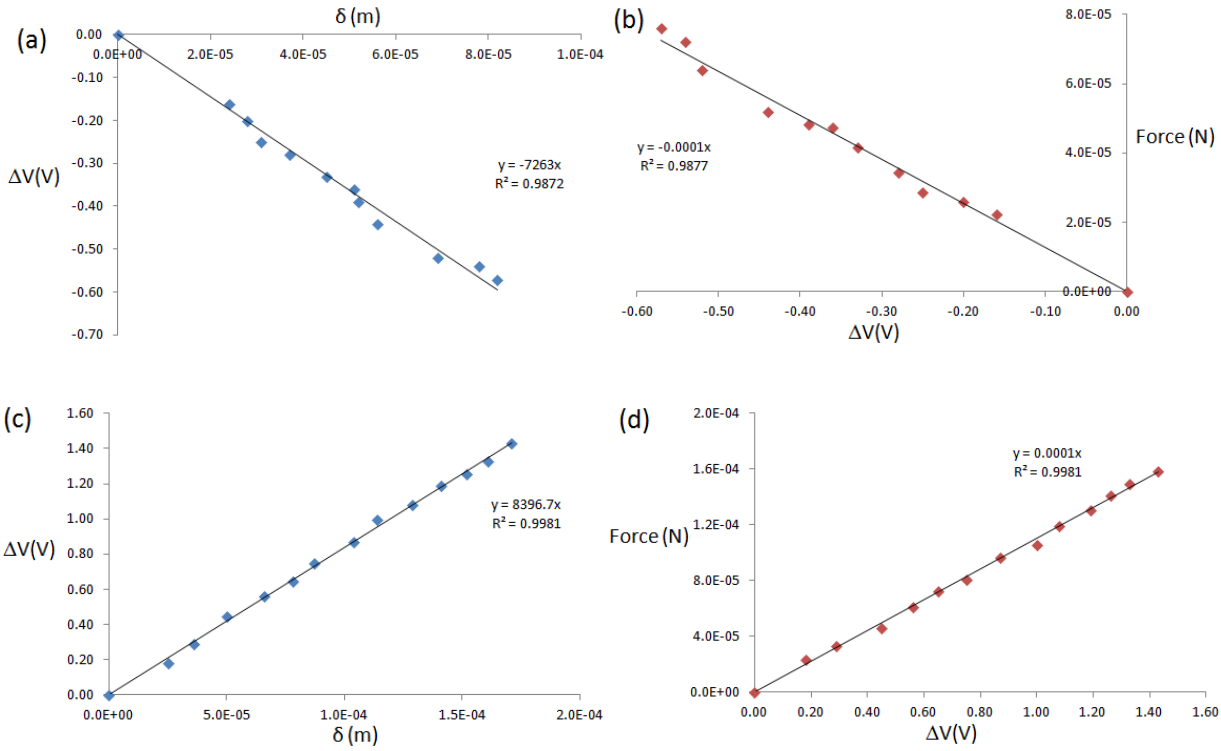

Figure 4.15 Results of sensor calibration. (a) ΔV vs. δ plot in -*D* direction (b) F vs. ΔV plot in -*D* direction (c) ΔV vs. δ plot in +*D* direction (d) F vs. ΔV plot in +*D* direction

The fourth cantilever with stiffness of 3.438 Nm^{-1} was calibrated and is shown in Figure 4.16. The measurements and calculations are shown in Table 4.4 and the plots of sensor calibration are shown in Figure 4.17.

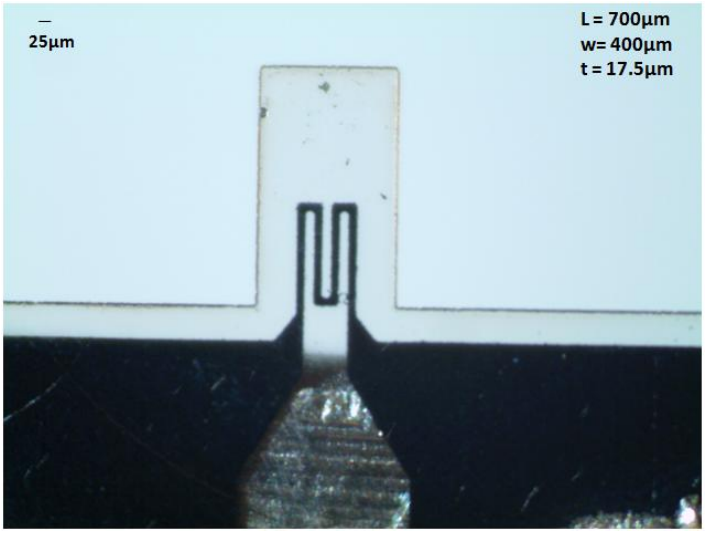

Figure 4.16 Microscopic image of cantilever with stiffness 3.438 Nm^{-1}

Table 4.4 Measurements and calculations of cantilever having stiffness 3.438 Nm^{-1}

R measured 4.33 KΩ	F_{max} (Theoretical) 129µN	F calculated from measured δ 388µN
Stiffness (Theoretical) 3.438 Nm^{-1}	δ_{max} (Theoretical) 37.5µm	δ measured 113µm

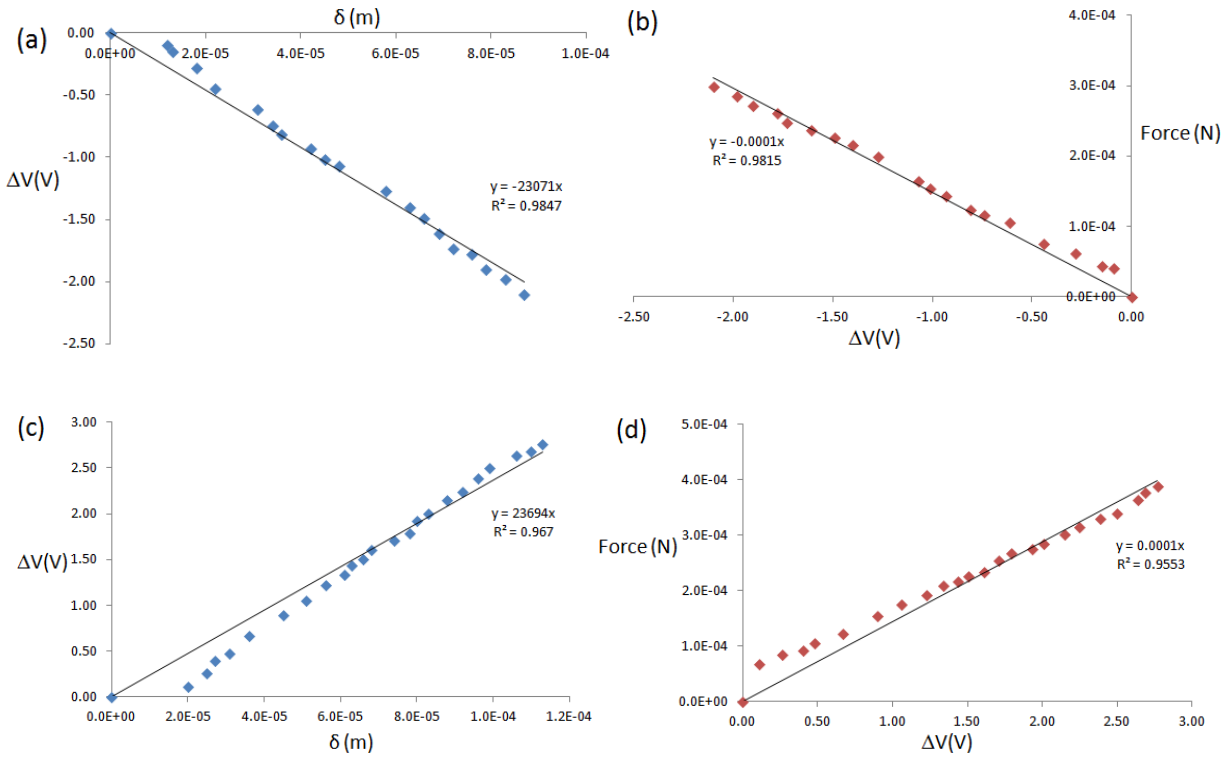

Figure 4.17 Results of sensor calibration. (a) ΔV vs. δ plot in *–D* direction (b) F vs. ΔV plot in *–D* direction (c) ΔV vs. δ plot in *+D* direction (d) F vs. ΔV plot in *+D* direction

4.3.2 Discussion

Four cantilevers with different dimensions and stiffness were calibrated. The results obtained were as expected. Stiffer the cantilever, large force can be detected with small deflection. Softer the cantilever, small force can be detected with large deflection. The maximum deflection measured under the microscope and the maximum force calculated from that deflection differed with the theoretical values 2-3 times. The theoretical maximum force and deflection was calculated using the maximum strain value of PVD chromium. The difference may be due to the yield strength value that is used to calculate the maximum strain of thin chromium film resistor. The magnitude can be of bulk chromium rather than a specific pattern

with very small thickness. The thickness of the thin chromium film resistor is around 50-70nm which is very small.

The first cantilever calibrated was the stiffest amongst all the cantilevers with a magnitude of 5.157 Nm^{-1}. The cantilever was deflected till 104µm detecting a force of 536µN. The measurements were 3 times the theoretical values. The cantilever was deflected to 170µm detecting a force of 908µN but when the cantilever was brought to its original position without deflection, the resistance of the thin chromium film resistor changed from 6.52 KΩ to 30 KΩ notifying the thin chromium film resistor broke. This happened when the cantilever was deflected about 5 times the theoretical value. Keeping this in mind, rest of the cantilevers were deflected 2-3 times the theoretical value which detected a force 2-3 times the maximum theoretical force of the cantilevers. When cantilevers were brought to their original position without deflection, the resistance of the thin chromium film resistors was the same as that was before calibration. The calibration results coincided with the theoretical values. The force range detected by the cantilevers was 5-500µN. The stiffness of the cantilever can be controlled by changing the dimensions of the cantilever. These cantilevers can be used for various applications that involve small force detection with large deflection and large force detection with small deflection.

4.4 Experiment to find the stiffness of elastic PDMS micro pillar

The purpose of this experiment was to realize cantilevers to manipulate an elastic micro structure mimicking cantilever manipulation with cluster of cells or cancer spheroid of comparable size. A PDMS film containing micro pillars of diameter 200µm and height 100µm was fabricated. The fabrication process is schematically shown below in Figure 4.18.

First a SU-8 mold was formed by UV lithography process. SU-8 2050 (MicroChem, USA) was spin coated on a glass substrate.

Program to spin coat 100µm SU-8 on glass substrate:

(Step1) Spin at 500 rpm for 10 seconds with acceleration of 100 rpm/second.

(Step2) Spin at 1750 rpm for 40 seconds with acceleration of 300 rpm/second.

After spin coating, the sample was soft baked at 97 degree Celsius for 15 minutes. Then the SU-8 layer was exposed to a pattern of UV light defined by a photomask. The photomask was designed on L-Edit. Post exposure bake was carried out for 9 minutes at 97 degree Celsius. Then the sample was developed using SU-8 developer for 9 minutes. The exposed part remains while the unexposed part goes away. Figure 4.19 shows a top view microscopic image of the SU-8 mold.

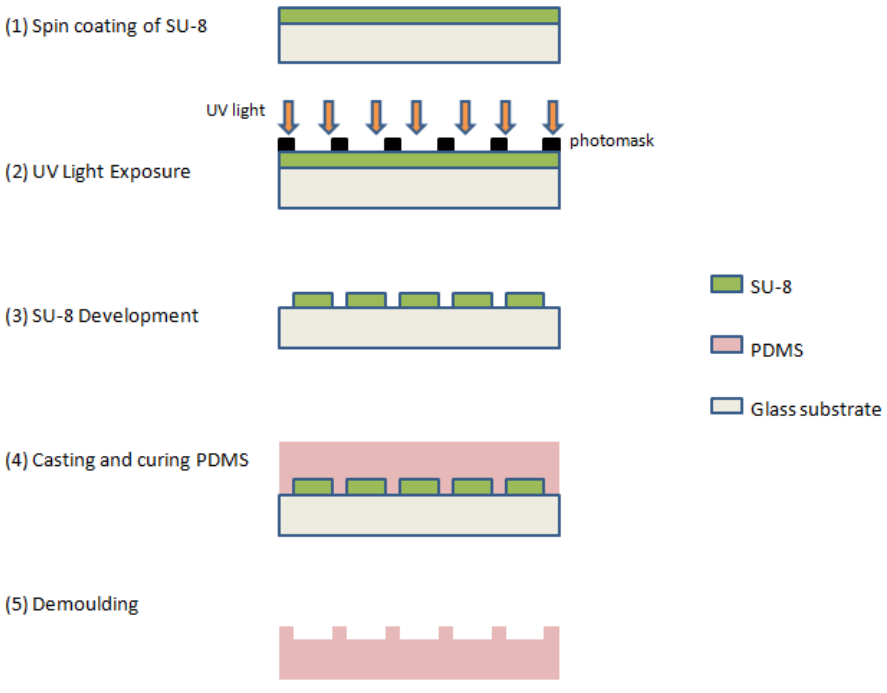

Figure 4.18 Schematic illustration for the fabrication of PDMS film with micro pillars

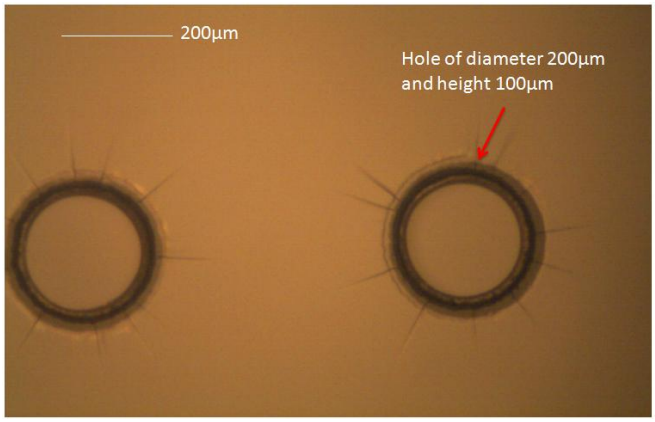

Figure 4.19 Microscopic image of SU-8 mold. It consists of a 100µm thick SU-8 layer on glass substrate, containing holes of diameter 200µm. There is no SU-8 in the holes

Then soft lithography was carried out. PDMS (Sylgard 184 Dow Corning) prepolymer and cross linker were mixed at a weight ratio of 10:1, degassed and cast into the SU-8 mold. PDMS was cured in an oven at 60 ^{o}C for 3 hours. In the last step, the PDMS film with an array of micro pillars was obtained after demoulding carefully from the SU-8 mold. Microscopic images of the PDMS film with an array of micro pillars having diameter 200µm and height 100µm are shown below in Figure 4.20.

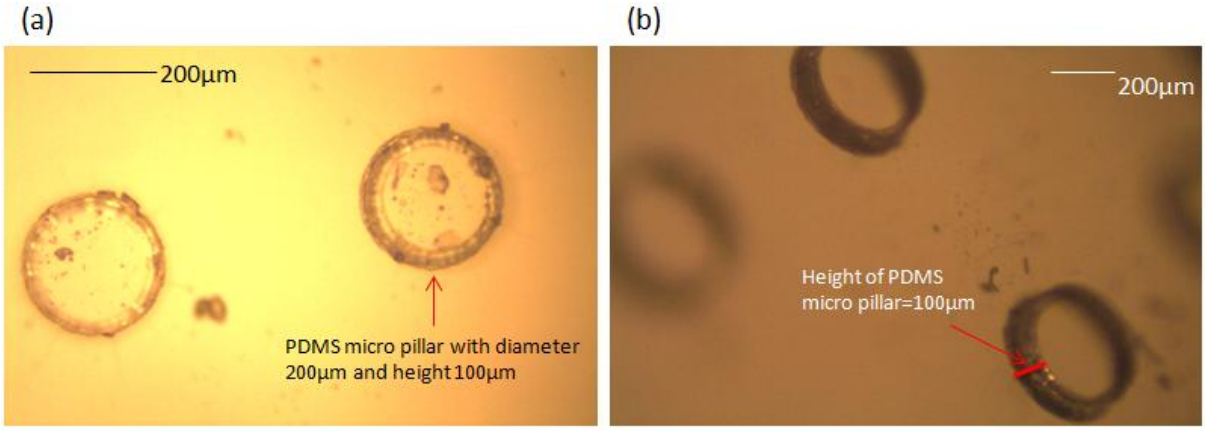

Figure 4.20 (a) Top view microscopic image of PDMS film with micro pillars (b) Angled view microscopic image of PDMS film with micro pillars

The experimental setup to find the stiffness of elastic PDMS micro pillar is shown below in Figure 4.21.

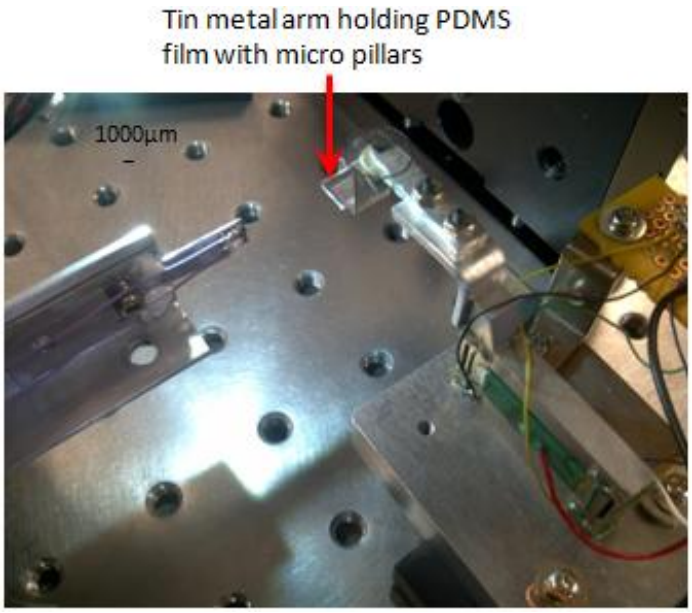

Figure 4.21 Experimental setup to find the stiffness of PDMS micro pillar

The experimental setup was the same as the setup used to calibrate the cantilevers except the piece of tin metal was replaced by a tin arm that can hold the PDMS film with micro pillars. The PDMS film was cut such that the cantilever could manipulate the micro pillars. The microscope images the top view of the PDMS film with micro pillars and side view of the cantilever. The mechanical stage was used to move the cantilever closer to the PDMS micro pillar. Figure 4.22 below shows the microscopic images of the experiment to find the stiffness of elastic PDMS micro pillar. Once it touched the micro pillar on one side, the mechanical stage was displaced in $-D$ direction as shown in Figure 4.22a, causing the cantilever to deflect at the free end and the elastic PDMS micro pillar was also displaced. In this case, the displacement of the mechanical stage is not equal to the cantilever deflection. Force (F) experienced at the free end causes deflection of the cantilever. The displacement of the mechanical stage and change in

voltage was measured. The mechanical stage was displaced until the cantilever deflected as shown in Figure 4.22b. The cantilever with stiffness 0.557 Nm^{-1} was used to find the stiffness of elastic PDMS micro pillar with diameter 200μm and height 100μm.

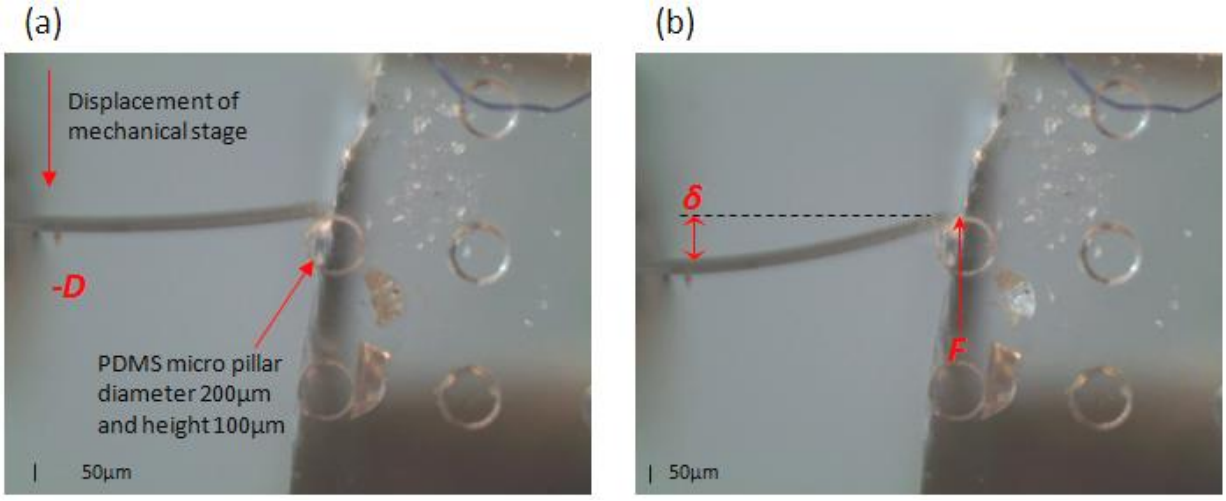

Figure 4.22 Microscopic images of cantilever manipulation to find stiffness of elastic PDMS micro pillar

4.4.1 Results

When the cantilever was moved against the PDMS micro pillar with the help of mechanical stage displacement, the cantilever deflected and the PDMS micro pillar displaced as well. In this case, the displacement of the mechanical stage is not equal to the deflection of cantilever as the PDMS micro pillar is elastic. The displacement of the mechanical stage is the sum of the cantilever deflection and the displacement of the PDMS micro pillar. The mechanical stage displacement and voltage was measured. The new voltage measurements gave new ΔV values. The displacement of the mechanical stage was plotted against ΔV and was compared with the plot from cantilever calibration as shown in Figure 4.23a. This showed the change in displacement and ΔV when cantilever was calibrated using tin metal and when the cantilever

deflected against elastic PDMS micro pillar. Using these new ΔV values, force (*F*) experienced at the free end was calculated by the relationship between *F* and ΔV from the cantilever calibration in Figure 4.13b. From these *F* values, the cantilever deflection was calculated (*F*=S.δ). The cantilever deflection was negated by the measured displacement of the mechanical stage giving the displacement of elastic PDMS micro pillar. The displacement of the elastic PDMS micro pillar was plotted against the force (*F*) as shown in Figure 4.23b. The slope of the plot gave the stiffness of the elastic PDMS micro pillar with diameter 200µm and height 100µm (*F*=S.δ).

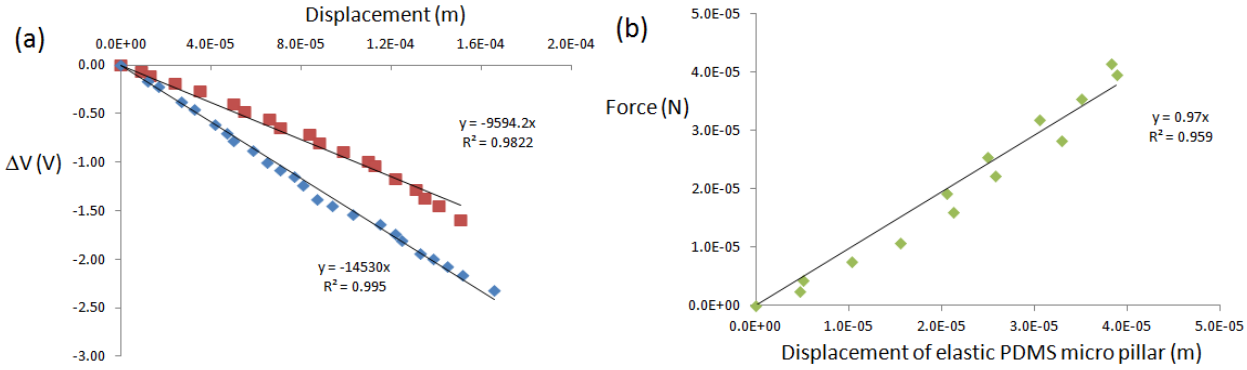

Figure 4.23 Results from experiment to find PDMS micro pillar stiffness

4.4.2 Discussion

The displacement of the mechanical stage was measured when the cantilever was calibrated and when the cantilever was used to find the stiffness of elastic PDMS micro pillar with diameter 200µm and height 100µm. Both were compared and shown in Figure 4.23a above. The blue line shows the plot from calibration and the red line shows the displacement of the mechanical stage and ΔV plot when the cantilever was used to find the PDMS micro pillar

stiffness. It could be estimated that the PDMS micro pillar was about 66 percent stiffer than the cantilever. The estimated stiffness of the micro pillar was 0.925 Nm^{-1}.

The force (F) experienced at the free end of the cantilever was plotted against the displacement of the elastic PDMS micro pillar as shown in Figure 4.23b. The slope of the plot gave the stiffness. The stiffness of elastic PDMS micro pillar with diameter 200μm and height 100μm was found to be 0.97 Nm^{-1} which was close to the estimated value. The results indicate that these cantilevers can be used to find stiffness of elastic micro scale structures.

4.5 Experiments to measure force in cancer cell manipulation

The purpose of these experiments was to show the capability of handling cells. To measure force in cancer cell manipulation, a cell holding device was fabricated. This cell holding device was a PDMS film that consisted of a circular well of depth 100μm and PDMS micro pillars with diameter 300μm and height 100μm. The circular well could hold cells and PDMS micro pillars were used as a supporting structure against which the aggregation of cancer cells could be manipulated by the cantilevers. The PDMS film was fabricated using the same fabrication process shown in Figure 4.18. First, a SU-8 mold was formed using UV lithography. Then soft lithography was carried out. PDMS was casted onto the SU-8 mold and cured. The PDMS film containing well and micro pillars was obtained after demoulding carefully from the SU-8 mold. Microscopic images of the PDMS film is shown below in Figure 4.24.

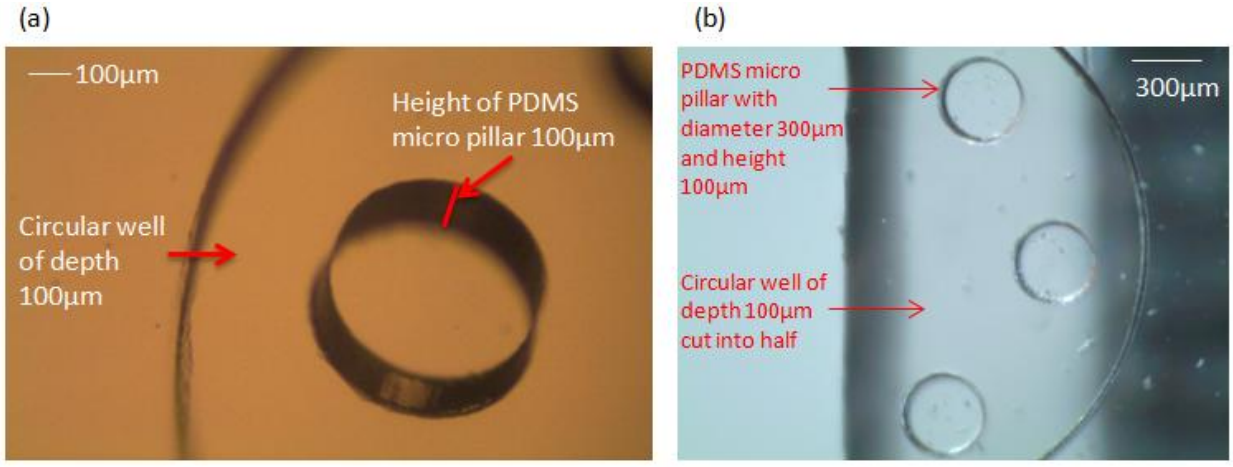

Figure 4.24 (a) Angled microscopic image of PDMS film containing circular well and PDMS micro pillars (b) Top view microscopic image used in experiment

The experimental setup to measure force in cancer cell manipulation was the same as the setup used to find the stiffness of elastic PDMS micro pillar. The tin metal arm holds the cell holding device (PDMS film). The circular well on the PDMS film was cut into half so that it allows the cantilever to manipulate the MCF-7 cells and micro pillars from the side. The PDMS film was then placed on the tin metal arm such that the microscope images the top view of the PDMS film as shown in Figure 4.24b and the side view of the cantilever. MCF-7 cancer cells were centrifuged and an aggregation of MCF-7 cancer cells was pasted onto the circular well of the PDMS film as shown below in Figure 4.25. The cantilever with stiffness 0.557 Nm^{-1} was used to measure force in cancer cell manipulation. After pasting the MCF-7 cancer cells onto the circular well of the PDMS film, using the displacement of the mechanical stage, the cantilever was moved and brought close to the MCF-7 cancer cells. Figure 4.25 below shows the microscopic images of the experiment to measure force in cancer cell manipulation. Once the cantilever touched the aggregation of MCF-7 cancer cells, the mechanical stage was displaced in $+D$ direction as shown in Figure 4.25a causing the cantilever to deflect at the free end. In this

case, the displacement of the mechanical stage is not equal to the cantilever deflection as MCF-7 cancer cells are elastic. Force (*F*) experienced at the free end causes deflection of the cantilever. The displacement of the mechanical stage and change in voltage was measured. The mechanical stage was displaced until the cantilever deflected as shown in Figure 4.25b.

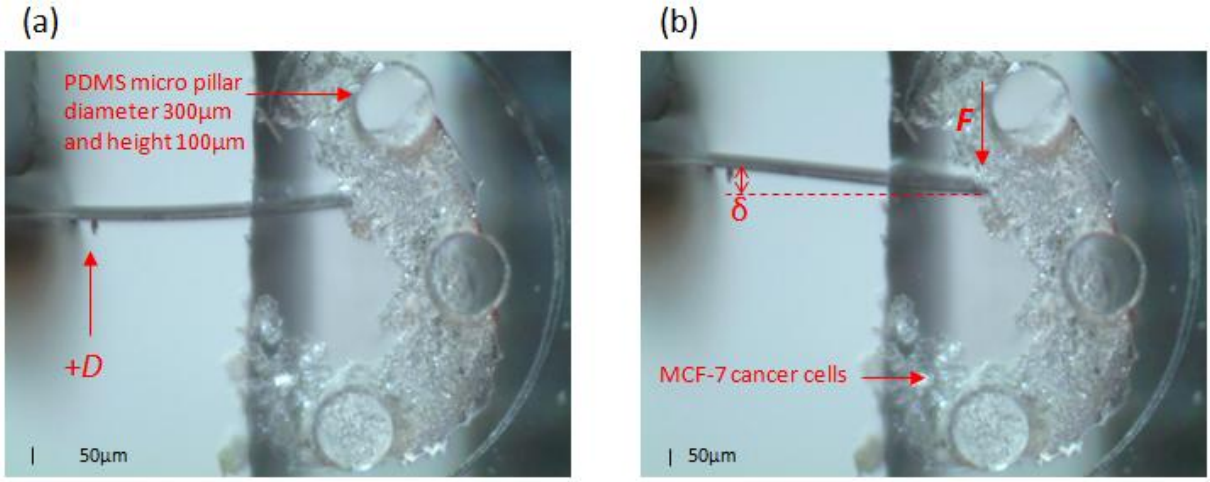

Figure 4.25 Microscopic images of Experiment1 to measure force in cancer cell manipulation

Another similar experiment was carried out to measure force in cancer cell manipulation and is shown in Figure 4.26 below.

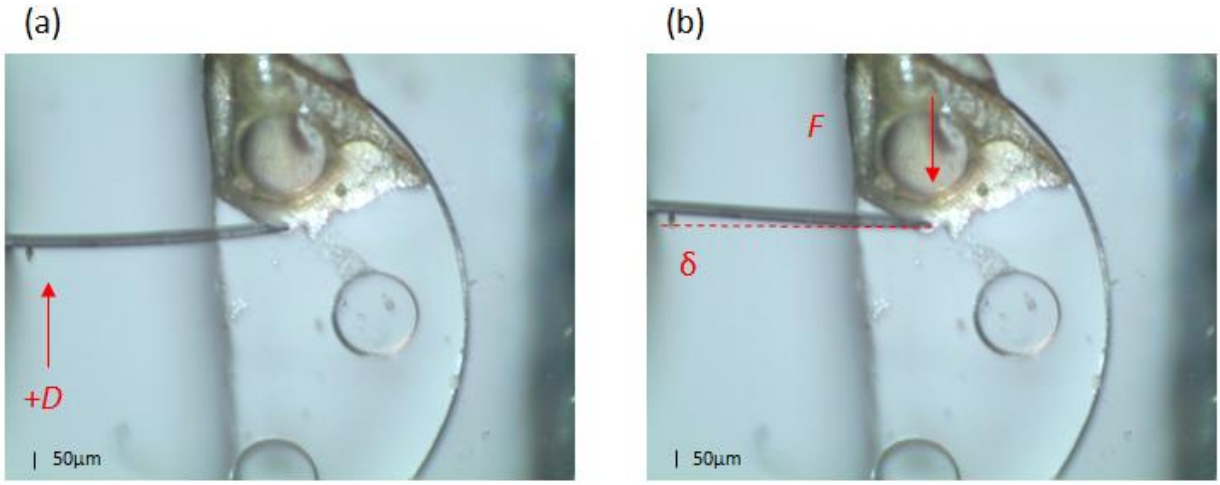

Figure 4.26 Microscopic images of Experiment2 to measure force in cancer cell manipulation

This time the aggregation of MCF-7 cancer cells was pasted and concentrated onto an elastic PDMS micro pillar of diameter 300μm and height 100μm.

4.5.1 Results

When the cantilever was moved against the aggregation of MCF-7 cancer cells in both experiments with the help of mechanical stage displacement, the cantilever deflected. In this case, the displacement of the mechanical stage is not equal to the deflection of cantilever as cancer cells are elastic. The displacement of the mechanical stage is the sum of the cantilever deflection and the indentation of aggregation of MCF-7 cancer cells caused by cantilever manipulation. In both experiments, the mechanical stage displacement and voltage was measured. The new voltage measurements gave new ΔV values. The displacement of the mechanical stage was plotted against ΔV and was compared with the plot from cantilever calibration as shown in Figure 4.27. Figure 4.27a shows the plot *D* vs. ΔV for experiment number 1 and 4.27b shows the *D* vs. ΔV plot for experiment number 2. This showed the change in displacement and ΔV when cantilever was calibrated using tin metal and when the cantilever deflected against the aggregation of MCF-7 cancer cells. Using these new ΔV values, force (*F*) experienced at the free end was calculated by the relationship between *F* and ΔV from the cantilever calibration. From these *F* values, the cantilever deflection was calculated (F=S.δ). The cantilever deflection was negated by the measured displacement of the mechanical stage giving the displacement of the system that consists of the PDMS film with PDMS micro pillars and aggregation of MCF-7 cancer cells. The displacement of system was plotted against the force (*F*) as shown in Figure 4.28. Figure 4.28a shows the plot of force (*F*) vs. displacement of system, for experiment number 1 and Figure 4.28b shows the plot of force (*F*) vs. displacement of system,

for experiment number 2. The slope of the plot gave the stiffness of the whole system that consists of the PDMS film with PDMS micro pillars and aggregation of MCF-7 cancer cells.

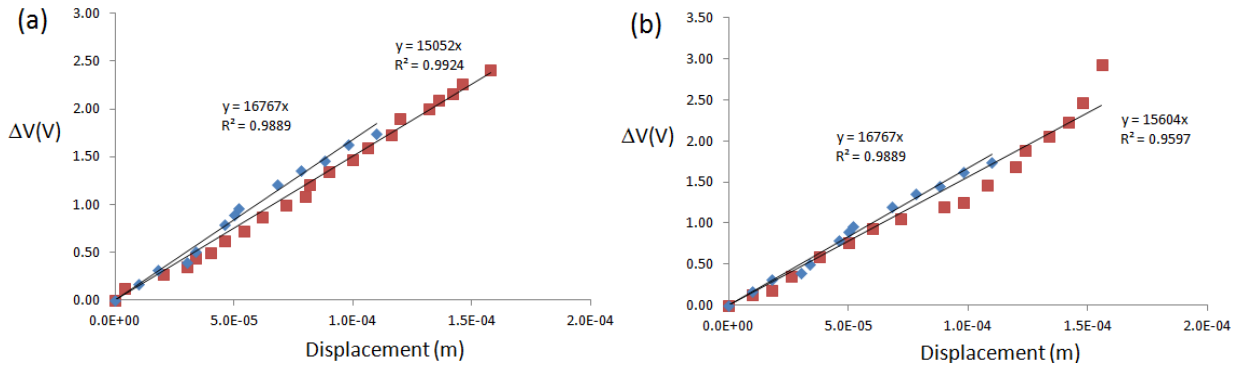

Figure 4.27 Displacement of mechanical stage vs. ΔV plots (a) Experiment1 (b) Experiment2

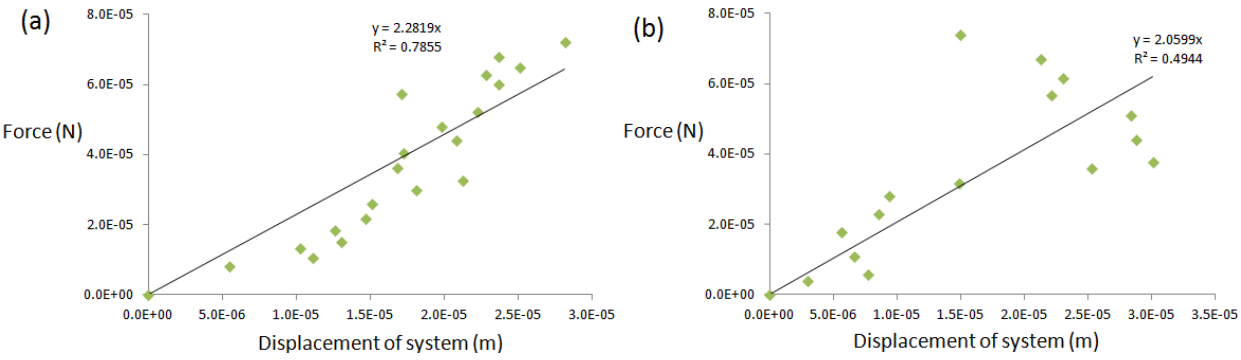

Figure 4.28 Force vs. Displacement of system (a) Experiment1 (b) Experiment2

4.5.2 Discussion

The purpose of these experiments was to show the capability of handling cells. The cantilever with least stiffness i.e. 0.557 Nm^{-1} was used to find the force measurements in cancer cell manipulation. This cantilever provided the least range of force used to manipulate the aggregation of cancer cells. The displacement of the mechanical stage was measured when the cantilever was calibrated and when the cantilever was used to measure force in cancer cell manipulation. Both were compared and shown for both experiments in Figure 4.27 above. The

blue lines show the plot from calibration and the red lines show the displacement of the mechanical stage and ΔV plot when the cantilever was deflected against the aggregation of MCF-7 cancer cells. The slopes in these graphs for both experiments were almost comparable. As mentioned, the circular well on the PDMS film was cut into half and used in Experiment 1. The other half was used in Experiment 2. In both Experiments, fresh aggregation of MCF-7 cancer cells was pasted onto the PDMS film. The comparable slopes show the cantilever deflected from an identical target structure in both experiments. The target structure was aggregation of MCF-7 cancer cells.

In Experiment 2, the mechanical stage was displaced till the cantilever deflected shown in Figure 4.26b. A force (*F*) range of 5-90μN was detected and applied on the aggregation of MCF-7 cancer cells. This force caused an indentation of aggregation of MCF-7 cancer cells which was seen under the microscope shown in Figure 4.29 below.

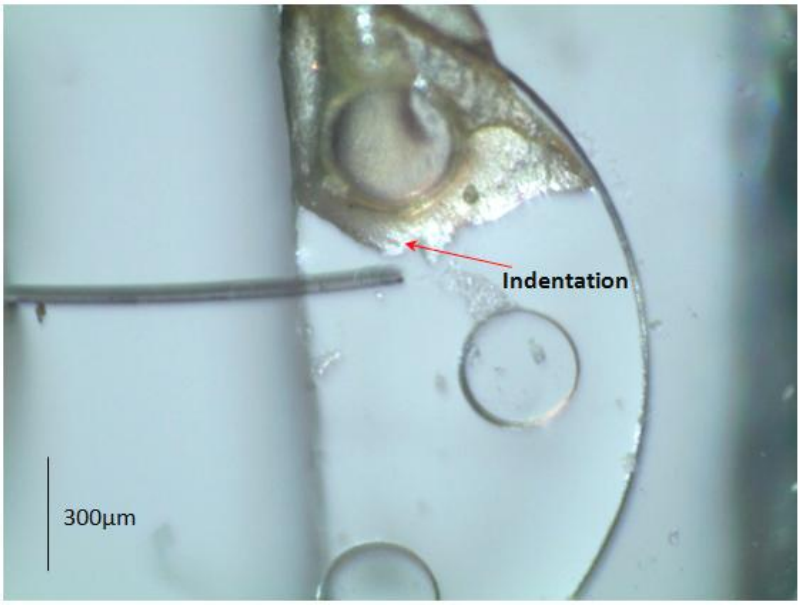

Figure 4.29 Indentation of aggregation of MCF-7 cancer cells caused by cantilever manipulation

Figure 4.28 above show the plots of force vs. displacement of system for both experiments. The slope of the plots gave the stiffness of the whole system that includes the PDMS film with PDMS micro pillars and aggregation of MCF-7 cancer cells. The measured stiffness in Experiment 1 was 2.28 Nm^{-1} and in Experiment 2 was 2.06 Nm^{-1}. The stiffness measurements are almost comparable. A measured range of 2.0-2.3 Nm^{-1} could be assumed of the stiffness of the whole system that consists of the PDMS film with PDMS micro pillars and aggregation of cancer cells.

These cantilever based sensors are compatible to explore the stiffness of cluster of cancer cells or cancer spheroids. Cancer model spheroids could be manipulated by the polymer micro scale force sensing cantilevers. Examining the stiffness of cluster of cancer cells may help understand the physical mechanisms involved in cancer metastasis and may help identify abnormal cell populations like tumors in detecting cancer.

These findings suggest that polymer based micro scale force sensing cantilevers designed, fabricated and tested in this study can be used for biosample manipulation and measurements.

Chapter 5

Conclusion

In this thesis, polymer based micro scale force sensing cantilevers were designed, fabricated and tested. SU-8 polymer was proposed as the cantilever material instead of traditional silicon technologies because it is difficult to fabricate cantilevers with sufficiently low stiffness to accomplish small forces required. Low Young's modulus of SU-8 constitutes low stiffness cantilevers which result in increased variation in cantilever deflection increasing the sensitivity of cantilevers. Micro fabrication technology was used to fabricate the polymer based cantilevers as it enables a versatile cantilever fabrication process allowing easy integration of additional functionality and variety of cantilever shapes to be designed. The cantilevers were integrated with thin chromium film resistors for sensor readout. Cantilever deflection induced stress on the surface of the cantilever changing the resistance of the thin chromium film resistor. A custom built amplifier allows for a sensitive response to the cantilever deflection. Thin chromium film resistors were proposed as thin metal film resistors because thin chromium film can be easily deposited using thermal evaporation. Chromium is readily available and inexpensive. The required thickness of thin metal film resistor deposited on the surface of the cantilever was very small and chromium provided a high resistivity compared to other metals.

Four cantilevers with different dimensions and stiffness were calibrated. The results obtained were as expected. Stiffer the cantilever, large force can be detected with small deflection. Softer the cantilever, small force can be detected with large deflection. The maximum deflection measured under the microscope and the maximum force calculated from that deflection differed with the theoretical values 2-3 times. The theoretical maximum force and

deflection was calculated using the maximum strain value of PVD chromium. The difference may be due to the yield strength value that is used to calculate the maximum strain of thin chromium film resistor. The magnitude can be of bulk chromium rather than a specific pattern with very small thickness. The calibration results coincided with the theoretical values. The force (*F*) range detected by the cantilevers was 5-500μN. The stiffness of the cantilever can be controlled by changing the dimensions of the cantilever allowing desired force range detection.

The cantilever based sensor was used to find the stiffness of an elastic PDMS micro pillar of diameter 200μm and height 100μm. The purpose of this experiment was to realize cantilevers to manipulate an elastic micro structure mimicking cantilever manipulation with cluster of cells or cancer spheroid of comparable size. A PDMS film containing micro pillars was fabricated using UV lithography and soft lithography techniques. When the cantilever was moved against the PDMS micro pillar with the help of mechanical stage displacement, the cantilever deflected and the PDMS micro pillar displaced as well. Using the measurements and calculations from cantilever calibration and cantilever manipulation with elastic PDMS micro pillar, the stiffness of an elastic PDMS micro pillar of diameter 200μm and 100μm was measured which was 0.97 Nm^{-1}.

The cantilever based sensor was also used to measure force in cancer cell manipulation. The purpose of this experiment was to show the capability of handling cells. A cell holding device was fabricated using UV lithography and soft lithography processes. The cell holding device was a PDMS film that consisted of a circular well of depth 100μm and PDMS micro pillars of diameter 300μm and height 100μm. MCF-7 cancer cells were centrifuged and pasted onto the circular well of the PDMS film. Using the measurements and calculations from cantilever calibration and cantilever manipulation with aggregation of cancer cells, the stiffness

of the whole system consisting of the PDMS film with PDMS micro pillars and aggregation of MCF-7 cancer cells was measured which was in the range 2.0-2.3 Nm^{-1}. A force range of 5-90μN was detected and applied which resulted in indentation of aggregation of MCF-7 cancer cells seen under the microscope.

These cantilever based sensors are compatible to explore the stiffness of cluster of cancer cells. Examining the stiffness of cluster of cancer cells may help understand the physical mechanisms involved in cancer metastasis and may help identify abnormal cell populations like tumors in detecting cancer. These findings suggest that polymer based micro scale force sensing cantilevers designed, fabricated and tested in this study can be used for biosample manipulation and measurements and a desired force range can be applied. These cantilevers can be used for various applications that involve small force detection with large deflection and large force detection with small deflection. Polymer based micro scale force sensing cantilevers can be used in micro fluidic applications as flow sensors. Other applications include molecule detection, material characterization and drug discovery.

5.1 Future directions

The cantilever based sensors designed, fabricated and tested in this study are compatible to explore the stiffness of cluster of cancer cells or cancer spheroid. Spherical cancer models have been used in cancer research. The study of cancer cells in a 3D context can provide insights not observed in conventional 2D monolayers. Spherical cancer models include multicellular tumor spheroids, tumorospheres, tissue-derived tumor spheres and organotypic multicellular spheroids (Weiswald et al., 2015). These models are formed by cell culture methods. The diameter of cancer spheroids range from 100μm to 600μm (West et al., 1989; Friedrich et al.,

2009; Dufau et al., 2012). Using the cell holding device, the polymer based micro scale force sensing cantilevers can be used to manipulate cancer spheroids and the stiffness of these cancer spheroids could be investigated.

References

Albrecht T, Akamine S, Carver T, Quate C. Micro fabrication of cantilever styli for the atomic force microscope. Journal of Vacuum Science & Technology A: Vacuum, Surfaces, and Films 1990; 8: 3386-96.

Binning G, Quate CF, Gerber C., "Atomic force microscope", Physical Review Letters 1986; 56: 930-3.

Boisen A, Dohn S, Keller SS, Schmid S, Tenje M, " Cantilever-like micromechanical sensors", Reports on progress in Physics 2011; 74: 036101.

Boisen A, Thaysen J, Jensenius H and Hansen O 2000 Environmental sensors based on micromachined cantilevers with integrated read-out Ultramicroscopy 82 11.

Carlson, R. H. G., C. V. Gabel, S. S. Chan, R. H. Austin, J. P. Brody, and J. W. Winkelman. 1997. Self-sorting of white blood cells in a lattice. Phys. Rev. Lett. 79:2149–2152.

S.L. Crick, F.C.P. Yin, Assessing micromechanical properties of cells with atomic force microscopy: importance of the contact point, Biomech. Model. Mechanobiol. 6 (3) (2007) 199–210.

S.E. Cross, Y.-S. Jin, J. Rao, J.K. Gimzewski, Nanomechanical analysis of cells from cancer patients, Nat. Nano. 2 (12) (2007) 780–783.

Isabelle Dufau, Céline Frongia, Flavie Sicard, Laure Dedieu, Pierre Cordelier, Frédéric Ausseil, Bernard Ducommun and Annie Valette, "Multicellular tumor spheroid model to evaluate spatio-temporal dynamics effect of chemotherapeutics: application to the gemcitabine/CHK1 inhibitor combination in pancreatic cancer", BMC Cancer 2012, 12:15 doi:10.1186/1471-2407-12-15.

Friedrich J, Seidel C, Ebner R, Kunz-Schughart LA: Spheroid-based drug screen: considerations and practical approach. Nat Protoc 2009, 4:309-24.

Jiali Gao; Le Guan; Jinkui Chu, "Determining the Young's modulus of SU-8 negative photoresist through tensile testing for MEMS applications", SPIE 7544, Sixth International Symposium on Precision Engineering Measurements and Instrumentation, 754464 (29 December 2010); doi: 10.1117/12.885983.

Genolet, G., Brugger, J., Despont, M. et al. (1999) Soft, entirely photoplastic probes for scanning force microscopy. Rev. Sci.Instrum. 70, 2398–2401.

J. Guck, S. Schinkinger, B. Lincoln, F. Wottawah, S. Ebert, M. Romeyke, D. Lenz, H.M. Erickson, R. Ananthakrishnan, D. Mitchell, J. Kas, S. Ulvick, C. Bilby, Optical deformability as an inherent cell marker for testing malignant transformation and metastatic competence, Biophys. J. 88 (5) (2005) 3689–3698.

Hochmuth, R. M. 2000. Micropipette aspiration of living cells. J. Biomech. 33:15–22.

M. Hopcroft, T. Kramer, G. Kim, K. Takashima, Y. Higo, D. Moore and J. Brugger, "Micromechanical testing of SU-8 cantilevers", 2005 Blackwell Publishing Ltd. Fatigue Fract Engng Mater Struct 28, 735–742.

Hopcroft, Matthew A.; Nix, William D.; Kenny, Thomas W. (2010), "What is the Young's Modulus of Silicon?", Journal of Microelectromechanical Systems 19 (2): 229.doi:10.1109/JMEMS.2009.2039697.

Hoyt K, Castaneda B, Zhang M, et al. Tissue elasticity properties as biomarkers for prostate cancer. Cancer biomarkers : section A of Disease markers. 2008;4(4-5):213-225.

A. Jemal, T. Murray, E. Ward, A. Samuels, R.C. Tiwari, A. Ghafoor, E.J. Feuer, M.J. Thun, Cancer statistics, 2005, CA Cancer J. Clin. 55 (1) (2005) 10–30.

T. A. Krouskop, T. M. Wheeler, F. Kallel, B. S. Garra, T. Hall. Elastic moduli of breast and prostate tissues under compression. Ultrason Imaging. 1998 October; 20(4): 260–274.

Kundu, T., J. Bereiter-Hahn, and I. Karl. 2000. Cell property determination from the acoustic microscope generated voltage versus frequency curves. Biophys. J. 78:2270–2279.

G.Y.H. Lee, C.T. Lim, Biomechanics approaches to studying human diseases, Trends Biotechnol. 25 (3) (2007) 111–118.

M. Lekka, P. Laidler, D. Gil, J. Lekki, Z. Stachura, A.Z. Hrynkiewicz, Elasticity of normal and cancerous human bladder cells studied by scanning force microscopy, Eur. Biophys. J. 28 (4) (1999) 312–316.

C.T. Lim, E.H. Zhou, A. Li, S.R.K. Vedula, H.X. Fu, Experimental techniques for single cell and single molecule biomechanics, Mater. Sci. Eng. C—Biomimetic Supramol. Syst. 26 (8) (2006) 1278–1288.

B. Lincoln, H.M. Erickson, S. Schinkinger, F. Wottawah, D. Mitchell, S. Ulvick, C. Bilby, J. Guck, Deformability-based flow cytometry, Cytometry A 59A (2) (2004) 203–209.

Mahaffy, R. E., C. K. Shih, F. C. MacKintosh, and J. Ka¨s. 2000. Scanning probe-based frequency-dependent microrheology of polymer gels and biological cells. Phys. Rev. Lett. 85:880–883.Kundu, T., J. Bereiter-Hahn, and I. Karl. 2000. Cell property determination from the acoustic microscope generated voltage versus frequency curves. Biophys. J. 78:2270–2279.

Maria Nordström, Stephan Keller, Michael Lillemose, Alicia Johansson, Søren Dohn, Daniel Haefliger, Gabriela Blagoi, Mogens Havsteen-Jakobsen and Anja Boisen, "SU-8 Cantilevers for Bio/chemical Sensing; Fabrication, Characterisation and Development of Novel Read-out Methods", Sensors 2008, 8, 1595-1612.

Rotsch, C., and M. Radmacher. 2000. Drug-induced changes of cytoskeletal structure and mechanics in fibroblasts: an atomic force microscopy study. Biophys. J. 78:520–535.

Sleep, J., D. Wilson, R. Simmons, and W. Gratzer. 1999. Elasticity of the red cell membrane and its relation to hemolytic disorders: an optical tweezers study. Biophys. J. 77:3085–3095.

S. Suresh, Biomechanics and biophysics of cancer cells, Acta Mater. 55 (12) (2007) 3989–4014.

O. Thoumine, A. Ott, Comparison of the mechanical properties of normal and transformed fibroblasts, Biorheology 34 (4–5) (1997) 309–326.

Wang, N., J. P. Butler, and D. E. Ingber. 1993. Mechanotransduction across the cell surface and through the cytoskeleton. Science. 260:1124–1127.

Ward, K. A., W. I. Li, S. Zimmer, and T. Davis. 1991. Viscoelastic properties of transformed cells: role in tumor cell progression and metastasis formation. Biorheology. 28:301–313.

Weiswald L-B, Bellet D, Dangles-Marie V. Spherical Cancer Models in Tumor Biology. Neoplasia (New York, NY). 2015;17(1):1-15. doi:10.1016/j.neo.2014.12.004.

West CM. Size-dependent resistance of human tumour spheroids to photodynamic treatment. British Journal of Cancer. 1989;59(4):510-514.

Wolter, O. and Bayer, Th. and Greschner J. Micromachined silicon sensors for scanning force microscopy. Journal of Vacuum Science & Technology B, 9, 1353-1357 (1991), DOI:http://dx.doi.org/10.1116/1.585195.

Zahalak, G. I., W. B. McConnaughey, and E. L. Elson. 1990. Determination of cellular mechanical properties by cell poking, with an application to leukocytes. J. Biomech. Eng. 112:283–294.

John X. J. Zhang and Kazunori Hoshino, "Molecular sensors and nanodevices, principles designs and applications in Biomedical Engineering", ISBN: 978-1-4557-7631-3 (2014).